Probabilistic Network Topology Prediction for Active Planning: An Adaptive Algorithm and Application

Liang Zhang, *Member, IEEE*, Zexu Zhang, Roland Siegwart, *Fellow, IEEE*, and Jen Jen Chung, *Member, IEEE*

***Abstract*—This article tackles the problem of active planning to achieve cooperative localization for multirobot systems under measurement uncertainty in GNSS-limited scenarios. Specifically, we address the issue of accurately predicting the probability of a future connection between two robots equipped with range-based measurement devices. Due to the limited range of the equipped sensors, edges in the network connection topology will be created or destroyed as the robots move with respect to one another. Accurately predicting the future existence of an edge, given imperfect state estimation and noisy actuation, is therefore a challenging task. An adaptive power series expansion (or APSE) algorithm is developed based on current estimates and control candidates. Such an algorithm applies the power series expansion formula of the quadratic positive form in a normal distribution. Finite-term approximation is made to realize the computational tractability. Further analyses are presented to show that the truncation error in the finite-term approximation can be theoretically reduced to a desired threshold by adaptively choosing the summation degree of the power series. Several sufficient conditions are rigorously derived as the selection principles. Finally, extensive simulation results and comparisons, with respect to both single and multirobot cases, validate that a formally computed and therefore more accurate probability of future topology can help improve the performance of active planning under uncertainty.**

***Index Terms*—Active planning under uncertainty, belief space, cooperative localization, disk communication model, GNSS-limited environment, probabilistic network topology.**

Manuscript received 11 October 2021; revised 24 April 2022; accepted 24 June 2022. This work was supported in part by the Basic Research Strengthening Program of China (173 Program) (2020-JCJQ-ZD-015-00), in part by the National Natural Science Foundation of China under Granted 61374213 and Grant 61573247, in part by the Open Foundation from Shanxi Key Laboratory of Integrated and Intelligent Navigation (SKLIIN-20180208), and in part by the scholarship from the China Scholarship Council. This article was recommended for publication by Associate Editor E. Montijano and Editor P. Robuffo Giordano upon evaluation of the reviewers' comments. *(Corresponding author: Zexu Zhang.)*

Liang Zhang is with the School of Engineering and Automation, Anhui University, Hefei 230601, China, with the Deep Space Exploration and Research Center, School of Astronautics, Harbin Institute of Technology, Harbin 150001, China, and also with the Autonomous System Lab, ETH Zürich, 8092 Zürich, Switzerland (e-mail: liangzhang@ahu.edu.cn).

Zexu Zhang is with the Deep Space Exploration and Research Center, School of Astronautics, Harbin Institute of Technology, Harbin 150001, China, and also with the Shaanxi Key Laboratory of Integrated and Intelligent Navigation, Harbin Institute of Technology, Harbin 150001, China (e-mail: zexuzhang@hit.edu.cn).

Roland Siegwart and Jen Jen Chung are with the Autonomous Systems Lab, ETH Zürich, 8092 Zürich, Switzerland (e-mail: rsiegwart@ethz.ch; jenjen.chung@mavt.ethz.ch).

Color versions of one or more figures in this article are available at https://doi.org/10.1109/TRO.2022.3189223.

Digital Object Identifier 10.1109/TRO.2022.3189223

I. Introduction

ACTIVE planning under uncertainty plays an important role for robots to autonomously navigate and operate in noisy environments by optimally choosing either systematic configurations or control inputs to minimize (or maximize) an aggregated objective function comprising various requirements from both task and safety needs. It has recently attracted more and more attention in a variety of applications in SLAM [1], sensor deployments [2], surveillance [3], search and rescue [4], etc.

It is a well-known problem in active planning under uncertainty that the planner cannot perfectly predict future measurements at planning time due to the existence of uncertainties from both motion and measurement processes. As a result, the planner cannot exactly evaluate the objective function given a control candidate. Typically, the measurement-related unknowns during planning include

1) The unknown distribution of raw measurement data from perceptive devices if a connection exists, and

2) A nondeterministic network of future measurements.

While the first is easily understood, the second one arises from the limited capacities of sensors, e.g., the range limitation of a radio device or field of view (FOV) of a camera as shown in Fig. 1. Since the future robot states are actually randomly distributed in uncertain scenarios, a measurement event in the future, i.e., the establishment of a measurement connection between two future nodes, is a random variable under the presence of limited sensing capacities. Therefore, the network topology of future measurements, which consists of all measurement events during the planning horizon, is nondeterministic at the planning time.

The problem of unknown future measurements during planning has been highlighted and partly relieved in some recent works [5]–[9]. However, the state-of-the-art works predict these future unknown variables only by some intuitive or experience-based methods. For example, the maximum likelihood (ML) assumption used in [5], wherein the future raw measurement data are simply determined by the prior estimates and therefore the distribution of future connection is calculated by the Bernoulli model. Besides, Indelman et al. [6] theoretically derived the expectation of the objective function over the unknown raw measurement data based on the one-step Gauss–Newton (GN) iteration process. However, the network of future measurement connections is still inherited and computed from the

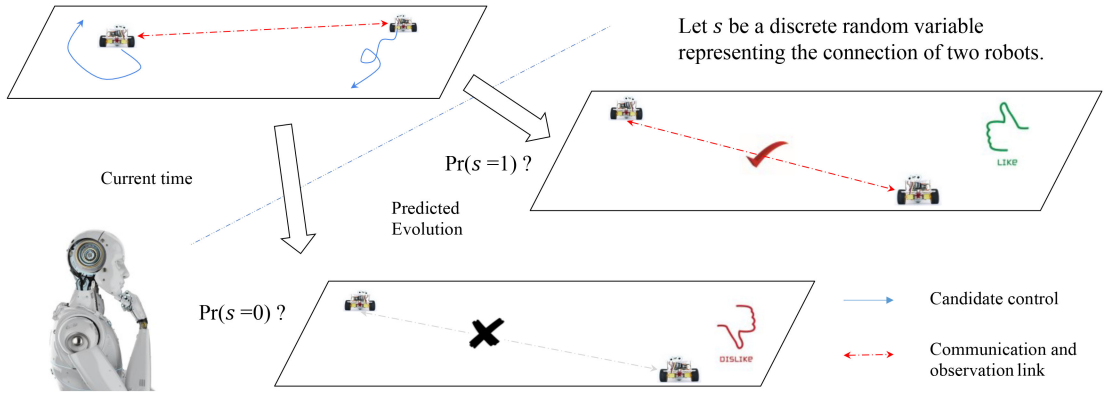

Fig. 1. Overall problem description of nondeterministic future network. A connection indicates a communication and (or) measurement event between the two associated nodes. Given robots' current states and a set of control candidates, the predicted evolution of future system behavior cannot fully determine future network within the planning horizon in a noisy environment.

ML assumptions. Pathak et al. [7] reasoned about the future data association problem in perceptually aliased environments, which is to identify the observed node if a future connection is established. However, once the data association is clear, then the raw measurement value is sampled from the propagated belief and the probability of this future connection is directly derived from a predefined and known Gaussian model. In addition, sampling-based methods and Gaussian models have also been applied in [8] and [9] to approximate these future variables.

The *key observation* in this work is that the performance of active planning can be improved if we can accurately predict the distributions of these future variables at planning time based on reasonable assumptions. To test such observation, we leave out the calculation of future raw data and concentrate on accurately predicting the distribution of future network connectivity. We mainly focus on a class of range-based communication and observation devices with maximum range threshold. An adaptive power series expansion (APSE) algorithm is developed in this article to predict the probability of each future measurement connection. Both theoretical analysis and numerical results are provided to guarantee the accuracy of APSE. It is then compared with several existing experience-based methods in two active planning scenarios, where robots are deployed to complete high-level tasks while localizing themselves. Numerical results show that an active planning framework using the APSE algorithm achieves more than 50% reduction over the localization uncertainty compared to using the Bernoulli model. The main contributions of this note are twofold:

1) APSE: to more accurately compute the exact probability of future connection between two nodes equipped with range-based communication and measurement devices given only current estimates and control candidates. Both theoretical guarantees and statistical validations are presented.

2) Extensive simulation results, showing that a more accurate event likelihood can indeed help improve the active planning performance.

We note that the first contribution is an extension of our previous work presented in [10]. Both papers apply the power series expansion formula of the quadratic positive form in a normal distribution from Provost and Mathai's lemma [11] to predict the probability of a measurement connection, wherein an infinite summation of series is required. In the previous work, we first take the finite-term approximation to realize computational tractability and then three more modifications are developed to tackle the truncation error introduced by omitting higher order terms. As further contributions, this article presents a rigorous theoretical analysis for the truncation error, by which we show that this error can be bounded by an arbitrary threshold if some sufficient conditions hold. These conditions are then summarized into the adaptive principles for the selection of the maximum power degree in the finite-term approximation. Besides, a new expansion method, termed as translational approximate covariance expansion (TRACE) is proposed for the singular cases where the covariance of the relative distance distribution is too small to stabilize the finite-term approximation.

II. Related Work

In this section, works most related to our approaches are discussed. The state of the art of three topics is presented with respect to the developments of belief space planning, connectivity control, and cooperative localization.

Belief Space Planning: Active planning performs sequential online decision making, which takes into account all the available information gathered up to the point each new decision is made.

Such problems can be efficiently solved as a Markov decision process (MDP) [12] or by dynamic programming (DP) methods [13]. However, early research mostly only considered systems with deterministic or finite state transition processes, which are feasible to solve in both computational complexity and optimality aspects.

In contrast, the active planning problem under uncertainty is often formulated under the POMDP framework due to the incorporation of uncertainties arising from both imperfect motion and noisy measurement. Belief space planning (BSP) methods are exactly an instantiation of a POMDP problem. Instead of planning in a configuration space where knowledge of the mean

of the estimated state distribution is sufficient for good performance, BSP optimizes the underlying problem in a continuous *belief space* by additionally taking the uncertainty of the state distribution (or belief, such as the covariance) into consideration.

Recent developments of BSP mainly focus on approximation methods in order to realize the balance of tractability and runtime complexity. These methods can be generally categorized into discrete and continuous groups according to the type of state space it considers. Discrete-domain planning, including point-based value iteration solvers [14], [15] and sampling-based methods [16]–[18], perform discretization over the belief space and hence generate a finite set of control candidates from which the optimal strategy is determined according to the maximum probability along each path (or equivalently the minimum uncertainty at the goal). Approaches in continuous spaces, optimized by a linear-quadratic Gaussian framework in belief space [5] or gradient descent [6], derive a locally optimal solution from a given initial plan that is generated from the discretized methods. More recently, some further improvements have contributed to reducing the computational complexity in large-scale deployments by leveraging the similarity between candidate actions for some specific forms of cost [19] and the recovery of future posterior covariance [20].

Connectivity Control: The problem of modeling and predicting network connectivity has been widely investigated in the area of wireless communication and *ad hoc* networks [21]. The preservation of connectivity is of great importance for packet routing, resource allocation, and bandwidth management, which have driven interest in the problem of connectivity control within the community. The connectivity of a system is often modeled as a proximity graph and thus the underlying problem is discussed with the help of graph theory. The Fiedler value of a graph or the second smallest eigenvalue of the Laplacian matrix of a graph is a concave function of the Laplacian matrix and implies network connectivity when it is positive definite [22]. Therefore, optimization-based connectivity controllers are designed through maximizing or minimizing the Fiedler value in either centralized [23] or distributed applications [24], [25].

Another prevailing methodology is the gradient-based potential field methods, which exploit the graph Laplacian matrix to construct a convex potential function and treat the loss of connectivity as obstacles in free space [26], [27]. As the aforementioned theories only consider proximity-based communication models composed of disk-based or uniformly fading-signal-strength communication links, more complex or realistic configurations have been further investigated to evaluate the effectiveness of multipath fading, intermittent or recurrent communication constraints, various communication models and so on [28], [29].

Besides, recent developments of connectivity research have extended far beyond its basic concept as just a medium of information transmission. The significance of connectivity is no longer only about the routing of information in a network, instead the underlying applications of relative observation as properties of communication links, such as the strength of signal (SOS) or time-of-flight (TOF), have been widely introduced for solving navigation and localization problems.

The differences between the traditional connectivity problem and the measurement event considered in this article can be distinguished in two aspects. First, despite the great success in connectivity control, most existing approaches rely on perfect knowledge of the sensor state, which is unavailable for real deployments in uncertain environments, such as GNSS-limited areas. Here, the future measurement event between two adjacent nodes is stochastic due to the presence of various uncertainties. Second and most important, the problem of predicting the existence of a future measurement event, which we consider in this article, only takes the change in system connectivity as an intermediate tool for achieving final objectives, while the traditional connectivity control problem only targets a desired network topology through their designed methods.

Cooperative Localization: Reliable relative observations enable the promising paradigm of using cooperative localization (CL) to navigate a multirobot system (MRS) through challenging environments.

In contrast to landmark-based localization methods, e.g., the typical framework of simultaneous localization and mapping (SLAM), CL depends little on the environment representations and hence is of potential advantage to be applied in more critical situations, for example, GNSS-limited areas such as in deep ocean or outer space.

Early on, the performance of CL has been studied as the problem of sensor deployment through both theoretical analysis [30], [31] and experimental validation [32], [33]. Using the centralized EKF as the engine of fusing measurements collected from the network, it has already been shown that, when the absolute position measurement is available, i.e., at least one robot can get a GNSS signal or measurements from an anchor, then the CL system is observable and the upper bound of steady-state location uncertainty is constant. The solution quality becomes independent of the initial uncertainty and is only dependent on the topology of the relative position measurement graph, and the accuracy of the proprioceptive and exteroceptive sensors of the robots. Recent research on CL arising from the field of wireless communication takes the exact radio model of the observation process into consideration, simultaneously considering the impacts from multipath propagation, transmitting power, clock delay, etc. [34], [35]. Collecting both sensor positions and the parameters of the communication channels into the joint estimated state and based on the Fisher information matrix (FIM), the authors proposed the equivalent FIM (EFIM) by extracting the subset of the FIM corresponding to the position states via the Schur complement operation [36]. As a result, the inverse of the trace of the EFIM, which is named the square position error bound (SPEB), can indicate the lower bound of the estimated sensor position error under the current network configuration.

Active planning of both configurations and motion strategies for CL in MRS is more critical and necessary than for the localization of a single robot. The main reason is that relative measurements contribute the only location information source to correct localization uncertainty in MRS. In contrast, there may be several possible options for single robot

applications. For example, in active SLAM, different loop closures can be selected and formed by reobserving different landmarks to reduce the uncertainty [1]. Research on network optimization includes optimal formation in [2], motion strategies in [37], and sensing frequency in [38]. The SPEB indicator-based active operations of the network are investigated in [39] with respect to the problems of node prioritization, sequential node activation, node deployment, and power allocation, etc. When uncertainties from both motion and measurement processes are considered, the optimal motion strategies for MRS have been studied in the contexts of target tracking, information gathering [3], active SLAM [1], and autonomous navigation [40] or coverage [41]. As a good combination, the BSP framework has been applied to the generation of control inputs of MRS while CL is activated for positioning robots in [42] and [43].

III. Preliminaries and Problem Formulation

A. General Notations

In this article, the notation $\mathbb{N}^+$ is used for the set of all positive integers. Given an integer $Z > 0$, we denote the set of all the positive integers no greater than Z as $\mathbb{N}_Z^+ := \{1, 2, \ldots, Z\}$. The notation $\mathbb{R}^n$ represents the vector space with dimensionality n while $\mathbb{R}^{n\times m}$ is the matrix space whose element size is $n \times m$. The operator $|\cdot|$ returns the absolute value of a scalar. The double-colon : used between two superscripts or subscripts represents a subset of consecutive elements, for example, $\boldsymbol{A} \in \mathbb{R}^n := \{a_1, a_2, \ldots, a_n\}$, then we have $\boldsymbol{A}_{2:5} = \{a_2, a_3, a_4, a_5\}$.

B. Configurations and Graph Theory

Consider a MRS composed of N identical robots operating in a GNSS-limited environment. We further suppose that the movement and measurement processes all suffer from stochastic noise. Let $\boldsymbol{p}_i^k$ and $\boldsymbol{W}_j$ denote the ith robot state at time step k and the jth assistant node state, respectively. All robots can only get their initial states and then need to cooperatively localize themselves using observations collected by the sensors and messages exchanged within the MRS. The assistant node state considered here may describe the positions of either landmarks (which remain static and unknown) or anchors (whose global positions are exactly known), which are observed by robots. While landmarks are generally used in the SLAM literature, anchors are often introduced in cases where specialized robots can occasionally get access to their exact position or when base stations are deployed in the environment broadcasting their global positions to nearby robots. Since landmarks can be categorized and formulated as special robots who do not suffer from motion noise and whose control inputs are always zeros, without loss of generality, we assume all assistant nodes are represented by anchors in this article for simplicity, whose number is denoted by M. In the following, we intermittently use "nodes" to represent robots or anchors.

Graph Theory: Assume all robots and anchors are associated with the nodes of a time-varying network topology graph $\mathcal{G}^k = \{\mathcal{V}, \mathcal{E}^k\}$ where $\mathcal{V}$ and $\mathcal{E}^k$ are the set of graph vertices and edges at time step k, respectively. The i-th node in the graph is denoted by $v_i, i \in \mathbb{N}_{M+N}^+$ as a result $\mathcal{V} := \{v_i | i \in \mathbb{N}_{M+N}^+\}$. In addition, the set of vertices $\mathcal{V}$ can be further divided into the subset of robots $\mathcal{V}_R$, and anchors $\mathcal{V}_A$, where $\mathcal{V}_R \cup \mathcal{V}_A = \mathcal{V}$. An edge between nodes v_i and v_j at time step k is denoted by $s_{i,j}^k = 1$ if they can mutually observe and communicate with each other, and $s_{i,j}^k = 0$ if not. Therefore, the subgraph among robots is undirected, i.e., $s_{i,j}^k = s_{j,i}^k, \forall i, j \in \mathcal{V}_R$. However, the edge only exists from robots to anchor, and not the other way around. The edge set is then defined as $\mathcal{E}^k := \{v_i \times v_j \in \mathcal{V}_R \times \mathcal{V} | s_{i,j}^k = 1\}$. The neighboring set $\boldsymbol{N}_i^k$ includes all the nodes v_j such that $s_{i,j}^k = 1$, i.e., $\boldsymbol{N}_i^k := \{v_j | s_{i,j}^k = 1\}$ and its size is denoted by n_i^k. In the following, an edge s_{ij}^k and the edge set $\mathcal{E}^k$ would be also referred to as the *connection* and the network topology, respectively. Furthermore, the node v_i is simply denoted by its index i and $i \in \mathcal{V}$ can implicitly denote all nodes in the environment, including both robots and anchors. Given the aforementioned scenario, if the planning horizon is L, then the number of future possible network topologies N_{con} can be calculated by $N_{con} = 2^{N_s}, N_s = \frac{L(M+N)(M+N-1)}{2}$.

C. Problem Formulations and Notations

Given the notations in Table I, we consider the conventional state transition model with additive Gaussian noise

$$\boldsymbol{p}_i^{k+1} = f_i\left[\boldsymbol{p}_i^k, \boldsymbol{u}_i^k, \boldsymbol{w}_i\right] \tag{1}$$

where $\boldsymbol{w}_i \sim \mathcal{N}(\boldsymbol{0}, \boldsymbol{R})$ with known information matrices $\boldsymbol{R}$. We further denote the corresponding probabilistic term of (1) as $p\left(\boldsymbol{p}_i^{k+1} | \boldsymbol{p}_i^k, \boldsymbol{u}_i^k\right)$.

The observation model under investigation is slightly different from the prevailing research in the presence of limited sensing capacity. We instead explicitly denote the output of the observation model by a 2-tuple $\boldsymbol{z}_{ij}^k :=< \vec{\boldsymbol{z}}_{ij}^k, s_{ij}^k >$. As earlier defined in the *Graph Theory* part, s_{ij}^k is a binomial random variable representing the existence of a connection between node i and j at time step k. $\vec{\boldsymbol{z}}_{ij}^k$ is the raw measurement data from a sensing device and is only valid when $s_{ij}^k = 1$, i.e.,

$$\vec{\boldsymbol{z}}_{i,j}^k = h_{ij}\left[\boldsymbol{p}_i^k, \boldsymbol{X}_j^k, \boldsymbol{v}_{i,j}\right] \tag{2}$$

where $\boldsymbol{v}_{i,j} \sim \mathcal{N}(\boldsymbol{0}, \boldsymbol{Q})$ with known information matrices $\boldsymbol{Q}$. The dimensionality of measurement $\vec{\boldsymbol{z}}_{i,j}$ is determined by the type of sensor. For example, $\vec{z}_{i,j}$ is a scalar if only the relative distance is observed by, for example, the radio sensor through measuring the TOF or SOS. $\vec{\boldsymbol{z}}_{i,j} \in \mathbb{R}^2$ if both distance and bearing are measured in radar.

Taking as an example the measurement of relative distance, which can be realized by, e.g., UWB, ultrasonic sensors, etc. If the real distance between any two nodes $i \in \mathcal{V}_R, j \in \mathcal{V}$ is

$$d_{i,j}(k) = \left\|\boldsymbol{p}_i^k - \boldsymbol{X}_j^k\right\|_2 \tag{3}$$

then given the maximum sensing radius ρ, the connection variable has

$$s_{i,j}^k = \begin{cases} 1, & d_{ij}(k) \le \rho \\ 0, & d_{ij}(k) > \rho \end{cases} \tag{4}$$

TABLE I
COLLECTION OF NOTATIONS AND THEIR DEFINITIONS.

Notation and definition	Descriptions
$\boldsymbol{X}^k := \{\boldsymbol{p}_1^k, \cdots, \boldsymbol{p}_N^k\}$	Set of all robot states at kth time step
$\boldsymbol{X}^{k_1:k_2} := \{\boldsymbol{X}^{k_1}, \cdots, \boldsymbol{X}^{k_2}\}$	Set of all robot states between time k_1 and k_2
$\boldsymbol{Z}_i^k := \{\boldsymbol{z}_{i,j}^k \vert \forall v_j \in \boldsymbol{N}_i^k\} = \{\vec{\boldsymbol{Z}}_i^k, \boldsymbol{N}_i^k\}$	Set of measurements for robot i at time k
$\mathscr{E}^k := \boldsymbol{N}_1^k \bigcup \boldsymbol{N}_2^k \bigcup \cdots \bigcup \boldsymbol{N}_N^k$	The communication and observation network of system at time k
$\boldsymbol{Z}^k, \boldsymbol{Z}^{k_1:k_2}, \boldsymbol{U}^k, \boldsymbol{U}^{k_1:k_2}, \mathscr{E}^{k_1:k_2}$	The same definitions as $\boldsymbol{X}^k$ and $\boldsymbol{X}^{k_1:k_2}$
$\boldsymbol{W} := \{\boldsymbol{W}_1, \cdots, \boldsymbol{W}_M\}$	Set of states for all anchors in environment
$[\boldsymbol{XW}]^k := \{\boldsymbol{X}^k, \boldsymbol{W}\}$	Set of states for all nodes in environment at time k
$\boldsymbol{X}_j^k \in [\boldsymbol{XW}]^k$	Single node state that can indicate either robots or anchors
$\mathscr{H}^{0:k} := \{\boldsymbol{Z}^{0:k}, \boldsymbol{U}^{0:k-1}, \boldsymbol{W}\}$	History data that have already been collected by time k
$\mathscr{H}^{0:k+l\vert k} := \{\mathscr{H}^{0:k}, \boldsymbol{U}^{k:k+l-1}\}$	History data with extra control candidates for the lth planning step.
$\boldsymbol{E} := \{\mathscr{E}_{iter}^{k+1:k+L} \vert \forall iter \in \mathbb{N}_{N_{con}}^+\}$	Set of all possible future connectivities during planning horizon L

and the raw measurement data has

$$\vec{\boldsymbol{z}}_{i,j}^k = d_{ij}(k) + v_{ij}, \quad v_{ij} \sim \mathcal{N}(0, Q). \tag{5}$$

We remark that the disk model is fairly standard in *ad hoc* networks, where all sensors are identical and of the same transmission power. Therefore, this model is commonly applied to represent range-based measurement and communication devices. Thus, the probabilistic term for the observation model $p\left(\boldsymbol{z}_{i,j}^k | \boldsymbol{p}_i^k, \boldsymbol{X}_j^k\right)$ can be decomposed as

$$\begin{aligned} p\left(\boldsymbol{z}_{i,j}^k | \boldsymbol{p}_i^k, \boldsymbol{X}_j^k\right) &= p\left(\vec{\boldsymbol{z}}_{i,j}^k, s_{ij}^k | \boldsymbol{p}_i^k, \boldsymbol{X}_j^k\right) \\ &= p\Big(\vec{\boldsymbol{z}}_{i,j}^k | \boldsymbol{p}_i^k, \boldsymbol{X}_j^k, s_{ij}^k = 1\Big) p\left(s_{ij}^k = 1 | \boldsymbol{p}_i^k, \boldsymbol{X}_j^k\right). \end{aligned} \tag{6}$$

We can write the posterior probability distribution function (pdf) over the joint state as

$$p\left(\boldsymbol{X}^{0:k} | \mathscr{H}^{0:k}\right). \tag{7}$$

Furthermore, given the prior distribution of robot states $p\left(\boldsymbol{p}_i^0\right), \forall i \in \mathcal{V}_R$, we can recursively expand the joint belief over system states by

$$\begin{aligned} b\left(\boldsymbol{X}^{0:k}\right) &= p\left(\boldsymbol{X}^{0:k} | \mathscr{H}^{0:k}\right) \\ &= \prod_{i \in \mathcal{V}_R} p\left(\boldsymbol{p}_i^0\right) \prod_{t=1}^{k} \left[p\left(\boldsymbol{p}_i^t | \boldsymbol{p}_i^{t-1}, \boldsymbol{u}_i^{t-1}\right) \prod_{j \in \boldsymbol{N}_i^t} p\left(z_{i,j}^t | \boldsymbol{p}_i^t, \boldsymbol{X}_j^t\right) \right]. \end{aligned} \tag{8}$$

If Gaussian noise is assumed, the belief can simply be denoted by a vector $\bar{\boldsymbol{X}}^{0:k}$ and a covariance (information) matrix $\boldsymbol{\Sigma}_{\bar{X}^{0:k}}^k$ representing the estimated means and uncertainties, respectively, i.e., $b\left(\boldsymbol{X}^{0:k}\right) = \mathcal{N}\Big(\bar{\boldsymbol{X}}^{0:k}, \boldsymbol{\Sigma}_{\bar{X}^{0:k}}^k\Big)$. In the estimation problem, the final purpose is to derive the optimal values of $\bar{\boldsymbol{X}}^{0:k}$ and $\boldsymbol{\Sigma}_{\bar{X}^{0:k}}^k$ using the available measurements, i.e., $\boldsymbol{Z}^{0:k}$ that has been collected from all sensors up to time k. Therefore, the connection variable in the estimation problem is deterministic and can be directly extracted from the collected data $\boldsymbol{Z}^{0:k}$ by

$$\begin{cases} s_{i,j}^t = 1, p\left(s_{i,j}^t = 1\right) = 1, & \text{if } \vec{z}_{ij}^t \in \boldsymbol{Z}^{0:k} \\ s_{i,j}^t = 0, p\left(s_{i,j}^t = 1\right) = 0, & \text{otherwise} \end{cases} \quad \forall t \le k \tag{9}$$

and the decomposition in (6) can be simplified as

$$p\left(z_{i,j}^t | \boldsymbol{p}_i^t, \boldsymbol{X}_j^t\right) = p\left(\vec{z}_{i,j}^t | \boldsymbol{p}_i^t, \boldsymbol{X}_j^t\right) \quad \forall \vec{z}_{i,j}^t \in \boldsymbol{Z}^{0:k}.$$

However, such simplification cannot be applied to the planning process since it lacks future measurement data. To highlight its impact on active planning, let us consider an expectation-based objective function J_k as

$$J_k\left(\boldsymbol{U}^{k:k+L-1}\right) = \mathop{\mathbb{E}}_{\boldsymbol{Z}^{k+1:k+L}} \left[\sum_{l=1}^{L} c^l\left(b\left(\boldsymbol{X}^{0:k+l}\right), \boldsymbol{U}^{k:k+l-1}\right) \right] \tag{10}$$

where the expectation operator $\mathbb{E}$ is taken with respect to the future observations of all robots, i.e., $\boldsymbol{Z}^{k+1:k+L}$. The reason for using the expectation here is that the future measurements are stochastic in the presence of uncertainties from both motion and observation noise. $c^l(\cdot)$ denotes an immediate cost function at the lth look-ahead step in terms of the joint belief $b\left(\boldsymbol{X}^{k+1:k+l}\right)$ and of the given control candidates. Traditionally, a motion policy from time k to $k+L$ is taken according to

$$\begin{aligned} {}^*\boldsymbol{U}^{k:k+L-1} &= \left\{{}^*\boldsymbol{U}^k, {}^*\boldsymbol{U}^{k+1}, \ldots, {}^*\boldsymbol{U}^{k+L-1}\right\} \\ &= \mathop{\arg\min}_{\boldsymbol{U}^{k:k+L-1}} \quad J_k\left(\boldsymbol{U}^{k:k+L-1}\right). \end{aligned} \tag{11}$$

Now, let us rewrite the expectation in (10) explicitly by recalling the composition of $\boldsymbol{Z}^{k+1:k+L} = \left\{\vec{\boldsymbol{Z}}^{k+1:k+L}, \mathscr{E}^{k+1:k+L}\right\}$ and applying the total probability over the future network and raw measurement data

$$\begin{aligned} &J_k\left(\boldsymbol{U}^{k:k+L-1}\right) \\ &= \int_{\vec{\boldsymbol{Z}}^{k+1:k+L}} \int_{\mathscr{E}^{k+1:k+L}} p\left(\vec{\boldsymbol{Z}}^{k+1:k+L}, \mathscr{E}^{k+1:k+L} | \mathscr{H}^{0:k+L|k}\right) \\ &\left[\sum_{l=1}^{L} c^l\left(\underbrace{p\Big(\boldsymbol{X}^{0:k+l} | \mathscr{H}^{0:k+l|k}, \vec{\boldsymbol{Z}}^{k+1:k+l}, \mathscr{E}^{k+1:k+l}\Big)}_{\mathrm{b}\left(\boldsymbol{X}^{0:k+l}\right)}, \boldsymbol{U}^{k:k+l-1} \right) \right] \\ &= \sum_{\mathscr{E}_{iter}^{k+1:k+L} \in \boldsymbol{E}} \underbrace{p\left(\mathscr{E}_{iter}^{k+1:k+L} | \mathscr{H}^{0:k+L|k}\right)}_{\text{term A}} \end{aligned}$$

$$\int_{\bar{\boldsymbol{Z}}^{k+1:k+L}} \underbrace{p\left(\bar{\boldsymbol{Z}}^{k+1:k+L}|\mathscr{H}^{0:k+L|k},\mathscr{E}_{iter}^{k+1:k+L}\right)}_{\text{term B}} \left[\sum_{l=1}^{L} \underbrace{c^l\left(\cdot\right)}_{\text{term C}}\right]. \tag{12}$$

The objective is composed of three terms. Term A is defined as network probability, which indicates how likely it is to form such a network during the planning horizon given the history data and the control candidates. Term B represents the likelihood of collecting a possible measurement from sensors when the network is specified. Remark that term B can be computed by the expansion in the estimation problem in (8) given the existence of future network. Then, the probability of raw measurement along each connection can be calculated by the measurement model as defined in (5). Term C is the immediate cost corresponding to the posterior probability of joint states from 0 to $k+l$ given a set of raw measurements and the network topology. It should at least concerns with the predicted uncertainty of future robot states.

It is clear that the network probability plays the role of weighting how much influence each future network branch can contribute to the objective function. Therefore, it is vital for the evaluation of the planning objective to accurately predict the network probability, instead of just using rough approximations as in existing works.

D. Spatial and Temporal Independence Assumption

Regarding the network probability (Term A), we can proceed by marginalizing over all possible robot states and applying the chain rule, yielding

$$p\left(\mathscr{E}_{iter}^{k+1:k+L}|\mathscr{H}^{0:k+L|k}\right) = \int_{\boldsymbol{X}^{k+1:k+L}} p\Big(\mathscr{E}_{iter}^{k+1:k+L}|\boldsymbol{X}^{k+1:k+L},\mathscr{H}^{0:k+L|k}\Big)p\Big(\boldsymbol{X}^{k+1:k+L}|\mathscr{H}^{0:k+L|k}\Big). \tag{13}$$

The following takes the assumption that the measurement connections in future networks $\mathscr{E}^{k+1:k+L}$ are both temporally and spatially independent

$$p\left(\mathscr{E}^{k}\right) = \prod_{i\in\mathcal{V}_R}\prod_{j\in\boldsymbol{N}_i^k} p\left(s_{i,j}^k\right) \tag{14}$$

$$p\left(\mathscr{E}^{k:k+L}\right) = \prod_{t=l}^{L} p\left(\mathscr{E}^{k+t}\right). \tag{15}$$

Note that this is a common assumption in the field of planning under uncertainty [6], [9]. Such assumption originates from estimation problems, where the Markov assumption is widely applied such that the future does not depend on the past given the present. It defines the merit of completeness to the states of robots, which entails that knowledge of past states, measurements, or controls carry no additional information that would help us to predict the future more accurately. As the states are complete under this assumption, then the measurement at the current time is conditionally independent of the past and future robot states, i.e., $[\boldsymbol{XW}]^k$ is sufficient to predict the potentially noisy measurement $\boldsymbol{Z}^k$. In other words, the Markov assumption guarantees that measurements are temporally independent [44]. Furthermore, the measurements are also spatially independent if the basic functioning principle of the observation devices on each robot do not interfere with each other. The extension of such an assumption from estimation to planning has not been fully discussed in existing works. As this problem is beyond the scope of this article, we just take this assumption and leave the problem of investigating the exact relationship of the measurement connections during the planning session as an open problem for future research.

Based on the aforementioned assumption, the network probability is also independent from the history of data given the distribution of future states, which yields

$$\begin{aligned} &p\left(\mathscr{E}_{iter}^{k+1:k+L}|\mathscr{H}^{0:k+L|k}\right) \\ &= \int_{\boldsymbol{X}^{k+1:k+L}} p\big(\mathscr{E}_{iter}^{k+1:k+L}|\boldsymbol{X}^{k+1:k+L}\big)p\Big(\boldsymbol{X}^{k+1:k+L}|\mathscr{H}^{0:k+L|k}\Big) \\ &= \prod_{\forall s_{ij}^t\in\mathscr{E}^{k+1:k+L}} \int_{\boldsymbol{p}_i^t,\boldsymbol{X}_j^t} \Big[p\big(s_{ij}^t|\boldsymbol{p}_i^t,\boldsymbol{X}_j^t\big)\, p\left(\boldsymbol{p}_i^t,\boldsymbol{X}_j^t|\mathscr{H}^{0:k+L|k}\right)\Big]. \end{aligned} \tag{16}$$

As a result, the network probability can be partitioned according to every possible individual connection. The integral over future states actually indicates that the probability computation of a connection is conditioned on the full distribution of its adjacent nodes. Since the integral can be over any distribution of the joint states $\boldsymbol{X}^{k+1:k+L}$, similarly to [7], we use the propagated belief $b\left(\boldsymbol{X}^{k+1:k+L|k}\right)$ in the following sections as

$$b\left(\boldsymbol{X}^{k+1:k+L|k}\right) = \int_{\neg\boldsymbol{X}^{k+1:k+L}} b\left(\boldsymbol{X}^{0:k+L|k}\right) \tag{17}$$

$$b\left(\boldsymbol{X}^{0:k+L|k}\right) = b\left(\boldsymbol{X}^{0:k}\right) p\left(\boldsymbol{X}^{k+1:k+L}|\boldsymbol{X}^{k},\boldsymbol{U}^{k+1:k+L}\right). \tag{18}$$

Therefore, the remaining problem is as follows.

Connection probability problem (CPP): For a system equipped with range-based measurement devices and assuming Gaussian noise, accurately compute the probability of each future connection $s_{ij}^{k+t}, \forall i,j\in\mathcal{V}, \forall t\in\mathbb{N}_L^+$, i.e., $p\left(s_{i,j}^{k+t}=1\right)$, given the control candidate $\boldsymbol{U}^{k:k+L-1}$, current estimates $b\left(\boldsymbol{X}^{0:k}\right)$ and prior knowledge about the sensing principles in (3)–(5).

IV. APSE: Probability of a Connection

In this section, an adaptive power series expansion (APSE) algorithm is developed for the CPP. First, a basic lemma about the factorial of a positive integer $n\in\mathbb{N}^+$ is presented.

Lemma 1: Given a positive integer n, its factorial has $(\frac{n}{e})^n < n! < e(\frac{n}{2})^n$, where e is the natural constant.

Further, Provost and Mathai's lemma forms the basis of our main algorithm. We state the lemma below and refer interested readers to [11, Sec. 4.2, pp. 91–99] for the complete proof.

Lemma 2: Given the p-dimensional multivariate normal distribution $\boldsymbol{X} \sim \mathcal{N}_p(\boldsymbol{\mu}, \boldsymbol{\Sigma})$, $\boldsymbol{\Sigma} > 0$ and its quadratic form $Y = Q(\boldsymbol{X}) = \boldsymbol{X}^T \boldsymbol{A} \boldsymbol{X}, \boldsymbol{A} = \boldsymbol{A}^T > 0$, let $\boldsymbol{b} = \boldsymbol{P}^T \boldsymbol{\Sigma}^{-\frac{1}{2}} \boldsymbol{\mu}$ and $\boldsymbol{\lambda} = [\lambda_1, \ldots, \lambda_p]^T$ be the eigenvalues of $\boldsymbol{\Sigma}^{\frac{1}{2}} A \boldsymbol{\Sigma}^{\frac{1}{2}}$, i.e., $\boldsymbol{P}^T \boldsymbol{\Sigma}^{\frac{1}{2}} A \boldsymbol{\Sigma}^{\frac{1}{2}} \boldsymbol{P} = \text{diag}(\boldsymbol{\lambda})$, $\boldsymbol{P}^T \boldsymbol{P} = I$. Then the corresponding cumulative distribution function (CDF) of Y, that is, $p\{Y \leq y\}$, will be denoted by $F_p(\boldsymbol{\lambda}; \boldsymbol{b}; y)$ and it can be expanded as follows:

$$F_p(\boldsymbol{\lambda}; \boldsymbol{b}; y) = \sum_{w=0}^{\infty} (-1)^w c_w \frac{y^{\frac{p}{2}+w}}{\Gamma\left(\frac{p}{2}+w+1\right)}, \quad 0 < y < \infty \tag{19}$$

where the coefficients c_w is defined by

$$c_0 = exp\left(-\frac{1}{2}\sum_{j=1}^{p} b_j^2\right) \prod_{j=1}^{p} (2\lambda_j)^{-\frac{1}{2}}$$

$$c_w = \frac{1}{w} \sum_{r=0}^{w-1} d_{w-r} c_r, \quad w \geq 1 \tag{20}$$

and d_w is given by

$$d_w = \frac{1}{2} \sum_{j=1}^{p} \left(1 - w b_j^2\right) (2\lambda_j)^{-w}, \quad w \geq 1. \tag{21}$$

More in-depth theoretical analysis of computing the CDF of quadratic form in normal variables by series representations can be found in [45] and [46].

A. Modeling and Finite-Term Approximation

At planning time step k, for two arbitrary nodes in the scenario, we can extract their state distribution from the propagated belief $b\left(\boldsymbol{X}^{k+1:k+L|k}\right)$. Let us denote their true positions at time step $k+l$ under the control candidate as $\boldsymbol{p}_1, \boldsymbol{p}_2$. Then, if the estimator used for propagated belief $b\left(\boldsymbol{X}^{k+1:k+L|k}\right)$ is complete, the distributions of $\boldsymbol{p}_1, \boldsymbol{p}_2$ can be reasonably treated by two normal distributions $\bar{\boldsymbol{P}}_1 \sim \mathcal{N}_1(\boldsymbol{\mu}_1, \boldsymbol{\Sigma}_1)$ and $\bar{\boldsymbol{P}}_2 \sim \mathcal{N}_2(\boldsymbol{\mu}_2, \boldsymbol{\Sigma}_2)$, which can be extracted from the propagated belief $b\left(\boldsymbol{X}^{k+l}\right)$.

As a result, we know that the subtraction of $\bar{\boldsymbol{P}}_1$ and $\bar{\boldsymbol{P}}_2$ is also a normal distribution. If the two distributions of future robot positions are independent of each other, then subtraction has $\Delta\bar{\boldsymbol{P}} = \bar{\boldsymbol{P}}_1 - \bar{\boldsymbol{P}}_2 \sim \mathcal{N}_\Delta(\boldsymbol{\mu}_1 - \boldsymbol{\mu}_2, \boldsymbol{\Sigma}_1 + \boldsymbol{\Sigma}_2)$. Otherwise, let us denote their covariance $\boldsymbol{\Sigma}_{1,2}$, then the variance of subtraction is slightly different: $\Delta\bar{\boldsymbol{P}} = \bar{\boldsymbol{P}}_1 - \bar{\boldsymbol{P}}_2 \sim \mathcal{N}_\Delta(\boldsymbol{\mu}_1 - \boldsymbol{\mu}_2, \boldsymbol{\Sigma}_1 + \boldsymbol{\Sigma}_2 - 2\boldsymbol{\Sigma}_{1,2})$.

By denoting $\Delta\bar{\boldsymbol{P}} = [\Delta\bar{P}_x, \Delta\bar{P}_y]^T$, the square of the true distance $d_{12} = \|\boldsymbol{p}_1 - \boldsymbol{p}_2\|_2$ can be equally represented by a quadratic random variable $Y = Q(\Delta\bar{\boldsymbol{P}}) = \Delta\bar{P}_x^2 + \Delta\bar{P}_y^2 = \Delta\bar{\boldsymbol{P}}^T \boldsymbol{A} \Delta\bar{\boldsymbol{P}}$, where $\boldsymbol{A} = \boldsymbol{I}$.

Considering the future connection variable $s_{1,2}$ under a range-based communication and observation device, whose maximum range is ρ, the relationship between random variables Y and $s_{1,2}$ is

$$p\left(s_{1,2} = 1\right) = p\left(Y \leq \rho^2\right). \tag{22}$$

As a result, it is straightforward to use Theorem 2 with dimensionality $p = 2$ and input $y = \rho^2$ to predict the probability of connection between two nodes, given the estimates of the means and covariance matrices of both nodes. However, Theorem 2 needs to compute an infinite summation of power series terms, which is intractable for practical applications. One instinctive approach is to sum only a finite but sufficient number of terms. This means replacing (19) with

$$F_2(\boldsymbol{\lambda}; \boldsymbol{b}; y) = \sum_{w=0}^{w_m} (-1)^w c_w \frac{y^{w+1}}{\Gamma(w+2)}, \quad 0 < y < \infty \tag{23}$$

where w_m is a proper maximum degree that our algorithm must determine. However, this method will introduce errors to the calculation of F_p compared with the original infinite sum version in Theorem 2. Thus, the main difficulty that remains is how to maintain the balance between the tractability and probability accuracy of our algorithm. This tradeoff is determined by the choice of degree w_m, which will be the main focus of the following sections.

B. Stability Analysis

In this section, some theoretical analyses are discussed in terms of the truncation error to provide some insights on how to determine this key parameter w_m. After selecting an appropriate w_m, the error of the CDF introduced by the omission of higher order terms is

$$\Delta F_2(\boldsymbol{\lambda}; \boldsymbol{b}; y) = \sum_{w=w_m}^{\infty} (-1)^w c_w \frac{y^{w+1}}{\Gamma(w+2)}, \quad 0 < y < \infty. \tag{24}$$

Since $w+2$ is always a positive integer, the Gamma function used here is the factorial of $w+1$, i.e.,

$$\Delta F_2(\boldsymbol{\lambda}; \boldsymbol{b}; y) = \sum_{w=w_m}^{\infty} (-1)^w c_w \frac{y^{w+1}}{(w+1)!}. \tag{25}$$

As we can see from the right-hand side of (25), this error term is also an infinite summation of series. Nevertheless, we are going to show that the error can be arbitrarily reduced so long as the degree w_m is appropriately selected. For the simplicity of derivation, first, the coefficient d_w from Theorem 2 is shown to be bounded in the following corollary.

Corollary 1: Given the 2-D multivariate normal distribution $\boldsymbol{X} \sim N_2(\boldsymbol{\mu}, \boldsymbol{\Sigma})$, let $\boldsymbol{\lambda} = [\lambda_1, \lambda_2]^T$ be the eigenvalues of covariance $\boldsymbol{\Sigma}$ and $\boldsymbol{b} = \boldsymbol{P}^T \Sigma^{\frac{1}{2}} \boldsymbol{\mu} = [b_1, b_2]^T$, where $\boldsymbol{P}$ is the eigenvector matrix of $\boldsymbol{\Sigma}$. Then, if we have

$$\begin{cases} 2\lambda_j > 1 \\ w \geq \frac{1}{b_j^2} + \frac{1}{2\lambda_j - 1} \end{cases} \quad \forall j \in \{1, 2\} \tag{26}$$

the limit of series d_w computed according to (21) is finite, i.e.,

$$\lim_{w \to \infty} d_w = 0 \tag{27}$$

and we have a positive number $d^u > 0$ such that

$$|d_w| < d^u \quad \forall w \in \mathbb{N}^+.$$

Proof: The proof is given in Appendix A. ■

Hereafter, we create two new series $\tilde{c}_w$ and $\tilde{d}_w$, respectively, where $\tilde{d}_w$ is defined as

$$\tilde{d}_w := [d^u, d^u, \ldots, d^u]. \tag{28}$$

Let $\tilde{c}_0 = c_0$, the remaining terms of $\tilde{c}_w$ are again recursively computed by (20), i.e.,

$$\begin{aligned}\tilde{c}_0 &= c_0 = exp\left(-\frac{1}{2}\sum_{j=1}^{p} b_j^2\right)\prod_{j=1}^{p}(2\lambda_j)^{-\frac{1}{2}}\\ \tilde{c}_w &= \frac{1}{w}\sum_{r=0}^{w-1}\tilde{d}_{w-r}\tilde{c}_r, \quad w \geq 1.\end{aligned} \tag{29}$$

The idea behind this new series $\tilde{c}_w$ is to serve as an envelope of c_w. We note that the definition equation in (29) is implicit and vague to understand. Hence, an exact formula is developed in the following corollary to provide a recursive version of its computation and the relationship between c_w and $\tilde{c}_w$.

Corollary 2: The new series $\tilde{c}_w$ defined in (29) and (28), can be recursively computed by

$$\tilde{c}_{w+1} = \frac{d^u + w}{w+1}\tilde{c}_w \tag{30}$$

and it is an envelope of c_w in (20), i.e.,

$$|c_w| \leq |\tilde{c}_w| \quad \forall w \in \mathbb{N}^+. \tag{31}$$

Proof: The proof is given in Appendix B. ■

Moving on, let us denote a positive integer $D \in \mathbb{N}^+$ such that $d^u \leq D \leq d^u + 1$, then we further introduce a new series defined as

1) if $D = 1$

$$e_w^1 = \frac{c_w}{(w+1)} \quad \forall w \in \mathbb{N}^+. \tag{32}$$

2) if $D \geq 2$

$$e_w^D = \begin{cases} c_w & w \leq (D-2) \\ \frac{c_w}{\prod_{j=1}^{D}(w+2-j)}, & w \geq (D-1). \end{cases} \tag{33}$$

A fact about e_w^D is summarized in the following Corollary.

Corollary 3: Given a finite and positive integer D, the limit of $|e_w^D|$ is also finite, i.e.,

$$\lim_{w\to\infty} |e_w^D| = Const. \tag{34}$$

and its maximum is constrained by $|e_w^D| \leq \tilde{c}_{D-1}$.

Proof: The proof is given in Appendix C. ■

Finally, we can conclude our main results of the truncation error in (25) in the following Theorem.

Theorem 1: Given the 2-D multivariate normal distribution $\boldsymbol{X} \sim N_2(\boldsymbol{\mu}, \boldsymbol{\Sigma})$, let $\boldsymbol{\lambda} = [\lambda_1, \lambda_2]^T$ be the eigenvalues of covariance $\boldsymbol{\Sigma}$ and $\boldsymbol{b} = \boldsymbol{P}^T\Sigma^{\frac{1}{2}}\boldsymbol{\mu} = [b_1, b_2]^T$, where $\boldsymbol{P}$ is the orthogonal matrix composed of the eigenvectors of $\boldsymbol{\Sigma}$. Let us compute the series d_w according to (21) and denote a positive integer D satisfying $d_w \leq D \leq d_w + 1$. Suppose

$$2\lambda_j > 1 \quad \forall j \in \{1, 2\} \tag{35}$$

then the truncation error $\Delta F_2(\boldsymbol{\lambda}; \boldsymbol{b}, y)$ in (25) can be reduced to a given threshold $\delta f > 0$, i.e.,

$$\Delta F_2(\boldsymbol{\lambda}; \boldsymbol{b}, y) < \delta f \tag{36}$$

if the degree $w_m \in \mathbb{N}^+$ in (23) is selected as

$$\begin{cases} w_m \geq \frac{1}{b_j^2} + \frac{1}{2\lambda_j - 1} \quad \forall j \in \{1, 2\} \\ w_m \geq e^2 y + D \\ w_m \geq 3D - \ln\left(\frac{\delta f}{c_0 y^D}\right) - 1. \end{cases} \tag{37}$$

Proof: Based on Corollaries 1–3, we recall and expand the expression $\Delta F_2(\boldsymbol{\lambda}; \boldsymbol{b}, y)$ deriving

$$\begin{aligned}\Delta F_2(\boldsymbol{\lambda}; \boldsymbol{b}; y) &= \sum_{w=w_m}^{\infty}(-1)^w c_w \frac{y^{w+1}}{(w+1)!}\\ &\leq \sum_{w=w_m}^{\infty}\frac{|c_w|}{\prod_{j=1}^{D}(w+2-j)}\frac{y^{w+1}}{(w+1-D)!}\\ &\leq \sum_{w=w_m}^{\infty}|\tilde{e}_w^D|\frac{y^{w+1}}{(w+1-D)!}\\ &\leq \tilde{c}_{D-1}\frac{y^{w_m+1}}{(w_m+1-D)!}\left(1+\sum_{w=1}^{\infty}\frac{y^w}{\prod_{j=1}^{w}(w_m+1+j-D)}\right)\\ &< \tilde{c}_{D-1}\frac{y^{w_m+1}}{(w_m+1-D)!}\left(1+\sum_{w=1}^{\infty}\frac{y^w}{(w_m-D)^w}\right).\end{aligned} \tag{38}$$

On the one hand, the latest infinite summation term in $\Delta F_2(\boldsymbol{\lambda}; \boldsymbol{b}, y)$ can be scaled down to the Basel Problem. Let

$$\frac{1}{\left(\frac{w_m - D}{y}\right)^w} \leq \frac{1}{w^2} \tag{39}$$

then the infinite summation term in $\Delta F_2(\boldsymbol{\lambda}; \boldsymbol{b}; y)$ has

$$\left(1+\sum_{w=1}^{\infty}\frac{y^w}{(w_m-D)^w}\right) \leq \left(1+\sum_{w=1}^{\infty}\frac{1}{w^2}\right) = 1 + \frac{\pi^2}{6}. \tag{40}$$

Therefore, the requirement in (39) can be cast into

$$\begin{aligned}&\frac{1}{\left(\frac{w_m - D}{y}\right)^w} \leq \frac{1}{w^2} \Rightarrow \left(\frac{w_m - D}{y}\right)^k \geq w^2\\ &\Rightarrow \ln(w_m - D) - \ln(y) \geq \frac{2\ln(w)}{w}.\end{aligned} \tag{41}$$

It is clear that the maximum of $\frac{\ln(w)}{w}$ is $\frac{1}{e}$. Accordingly we need

$$\ln(w_m - D) - \ln(y) \geq \frac{2}{e} \Rightarrow w_m \geq e^{\frac{2}{e}}y + D. \tag{42}$$

On the other hand, let us denote $g(w_m) = \frac{y^{w_m+1}}{(w_m+1-D)!}$ and take a subtraction between $g(w_m)$ and $g(w_m + 1)$, which yields

$$\begin{aligned}&g(w_m+1) - g(w_m)\\ &= \frac{y^{w_m+2}}{(w_m+2-D)!} - \frac{y^{w_m+1}}{(w_m+1-D)!}\end{aligned}$$

TABLE II
VALUES OF w_m WHEN $g(w_m)$ IS LESS THAN A CERTAIN THRESHOLD GIVEN FINITE y AND D.

Conditions	$g(w_m) \leq$			
	10^{-3}	10^{-5}	10^{-10}	10^{-20}
y = 25(ρ = 5), D = 10	108	109	118	133
y = 25(ρ = 5), D = 20	139	141	149	163
y = 100(ρ = 10), D = 10	327	327	340	359
y = 100(ρ = 10), D = 20	375	378	387	405

$$= \frac{y^{w_m+1}}{(w_m+1-D)!}\left(\frac{y}{w_m+2-D}-1\right).$$

As a result, we know that $g(w_m)$ takes its maximum when $w_m = y+D-2$ or $w_m = y+D-1$, and that $g(w_m)$ is decreasing after $w_m > y+D-1$. Besides, its limit is exactly zero when the selected w_m tends to infinity.

Consequently, the error function is bounded by

$$\Delta F_2(\boldsymbol{\lambda}; \boldsymbol{b}; y) \quad < \tilde{c}_{D-1}\left(1+\frac{\pi^2}{6}\right) g(w_m). \tag{43}$$

We remark here that given finite y and D, the output of $g(w_m)$ decreases sharply after $w_m > y+D-2$. Table II gives the tendency of its decrement. Therefore, despite the value of $\tilde{c}_{D-1}$, we could just simply take a larger w_m to reduce the truncation error $\Delta F_2(\boldsymbol{\lambda}; \boldsymbol{b}; y)$ as $\tilde{c}_{D-1}$ is finite.

However, in contrast to our previous method of fixing the selected degree w_m beforehand, it would be more flexible to adaptively determine that degree online given the different distribution of relative distance between two nodes at each time. As a result, we need to dig into this error equation further to provide some insights on real-time access for the choice of such degree if a desired threshold δf of the truncation error is defined, i.e., find a proper w_m so that $\Delta F_2 < \delta f$.

Firstly, with the help of the recursive computation version of $\tilde{c}_w$ in (30), we can derive an explicit equation of $\tilde{c}_w$

$$\begin{aligned}\tilde{c}_k &= \frac{k-1+d^u}{k}\tilde{c}_{k-1} \\ &= \frac{\prod_{i=0}^{k-1}(d^u+i)}{\prod_{j=0}^{k-1}(j+1)}\tilde{c}_0.\end{aligned} \tag{44}$$

Since $d^u \leq D$, $\prod_{i=0}^{w-1}(d^u+i) \leq \prod_{i=0}^{w-1}(D+i) = \frac{(D+w-1)!}{(D-1)!}$, we therefore know that

$$\tilde{c}_w \leq \frac{(D+w-1)!}{k!(D-1)!}\tilde{c}_0 \quad \forall w \in \mathbb{N}^+ \tag{45}$$

and as a result

$$\tilde{c}_{D-1} \leq \frac{(2D-2)!}{(D-1)!(D-1)!}\tilde{c}_0 \tag{46}$$

then recalling Lemma 1 yields

$$\begin{aligned}\tilde{c}_{D-1} &\leq \frac{(2D-2)!}{(D-1)!(D-1)!}\tilde{c}_0 \\ &\leq \frac{e(D-1)^{2D-2}}{\left(\frac{D-1}{e}\right)^{D-1}\left(\frac{D-1}{e}\right)^{D-1}}\tilde{c}_0 \\ &\leq e^{2D-1}\tilde{c}_0 = e^{2D-1}c_0.\end{aligned} \tag{47}$$

Next, let us consider the term $g(w_m)$. If we denote $\alpha = w_m + 1 - D$, then $g(w_m) = \frac{y^{\alpha+D}}{\alpha!}$. Again, by recalling Lemma 1, we obtain

$$g(w_m) = \frac{y^{\alpha+D}}{\alpha!} \leq \frac{y^{\alpha+D}e^{\alpha}}{\alpha^{\alpha}} = \left(\frac{ye}{\alpha}\right)^{\alpha} y^D. \tag{48}$$

So if an error threshold δf is given, in order to limit the truncation error under such a value, we can set

$$\Delta F_2(\boldsymbol{\lambda}; \boldsymbol{b}; y) \leq e^{2D-1}c_0\left(1+\frac{\pi^2}{6}\right)\left(\frac{ye}{\alpha}\right)^{\alpha} y^D < \delta f. \tag{49}$$

Since $1+\frac{\pi^2}{6} < e$, the above requirement can be further rewritten as

$$e^{2D}\left(\frac{ye}{\alpha}\right)^{\alpha} < \frac{\delta f}{c_0 y^D}. \tag{50}$$

Let us denote $\tilde{g}(\alpha) = (\frac{ye}{\alpha})^{\alpha}$, then similar to the analysis of $g(k_m)$, it is easy to show that $\tilde{g}(\alpha)$ is monotonically decreasing when $\alpha \geq ey, \forall \alpha \in \mathbb{N}^+$. Therefore, we propose two stages to determine the proper degree α,

1) if $\alpha \geq e^2 y \Rightarrow w_m \geq e^2 y + D - 1$, then

$$e^{2D}\left(\frac{ye}{\alpha}\right)^{\alpha} \leq e^{(2D-\alpha)} \tag{51}$$

2) we can let $e^{(2D-\alpha)} < \frac{\delta f}{c_0 y^D}$, then

$$\begin{aligned}&\alpha > 2\mathrm{D} - \ln\left(\frac{\delta f}{c_0 y^D}\right) \\ &\Rightarrow w_m > 3\mathrm{D} - \ln\left(\frac{\delta f}{c_0 y^D}\right) - 1.\end{aligned} \tag{52}$$

Considering the conditions both in the Basel Problem (42) and in Corollary 1, we can summarize the set of sufficient conditions as listed in (37). ■

C. Translational Approximate Covariance Expansion

Theorem 1 demonstrates that one can reduce the truncation error introduced by the finite-term approximation in (23) by increasing the selected degree w_m. The rules of determining w_m show its relationship between the shape of the covariance, the range limitation, and also the desired error threshold. It presents a guaranteed and numerically efficient computation method for the probability of connection. However, all aforementioned analyses are built upon a very important assumption in (35), that is, the proposed finite-time approximation can only be efficient when the given relative covariance is well-constructed, i.e., its eigenvalues are greater than $\frac{1}{2}$.

This is a very critical constraint since in real applications the robot beliefs continue to be updated after each new control action or whenever a new measurement is obtained. Demonstrated as the second disadvantage in our previous work [10], this constraint will cause fatal prediction failure when using the finite-term approximation in (23) for the case where the relative covariance is too small or near singularity and the relative distance of the two corresponding robots $d_{12} = \|\boldsymbol{p}_1 - \boldsymbol{p}_2\|_2$ is very close to the range threshold ρ.

Though this constraint is partly relieved by the approximate covariance expansion (ACE) proposed in our prior research,

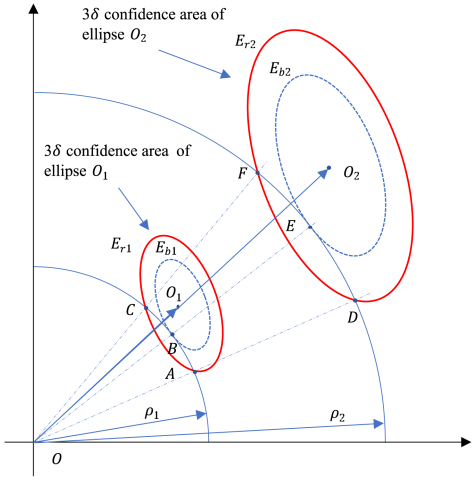

Fig. 2. Geometric illustration of TRACE.

Algorithm 1: TRACE.

Result: $\boldsymbol{\mu}_2, \boldsymbol{\Sigma}_2, \rho_2$;
Data: $\boldsymbol{\mu}_1, \boldsymbol{\Sigma}_1, \rho_1$;
$\lambda_{min} \leftarrow$ compute the minimum eigenvalue of $\boldsymbol{\Sigma}_1$;
if $\lambda_{min} < \frac{1}{2}$ **then**
  $\beta = \frac{1}{\lambda_{min}}$, $\boldsymbol{\Sigma}_2 = \beta\boldsymbol{\Sigma}_1$, $\boldsymbol{\mu}_2 = \sqrt{\beta}\boldsymbol{\mu}_1$, $\rho_2 = \sqrt{\beta}\rho_1$;
else
  $\boldsymbol{\Sigma}_2 = \boldsymbol{\Sigma}_1$, $\boldsymbol{\mu}_2 = \boldsymbol{\mu}_1$ $\rho_2 = \rho_1$;
end
Return $\boldsymbol{\mu}_2, \boldsymbol{\Sigma}_2, \rho_2$

ACE suffers from lots of approximations and hence the probability precision is corrupted and degenerated. Regarding these problems, we further propose an improved version of ACE, where the expansion is transitioned to a new and collinear center instead of dilating the covariance at its ellipse center. This approach is hereafter called the translational approximate covariance expansion (TRACE). A geometric depiction of TRACE is shown in Fig. 2, where the red solid ellipse E_{r1} represents the 3δ confidence area corresponding to the covariance matrix $\Sigma = \Sigma_1 + \Sigma_2$ of $\Delta\bar{P}$. Taking the maximum range of the measurement device to be ρ_1, its ranging circle from the origin O with radius ρ_1 intercepts with the 3δ area of E_{r1}. There exists a smaller ellipse E_{b1} that is tangent to this ranging circle. Therefore, the probability $p(Y < \rho_1^2)$ can be indicated by

$$p\left(Y < \rho_1^2\right) = \frac{S(\widehat{ABC} \cap E_{r1})}{S(E_{r1})} \tag{53}$$

where $S(\cdot)$ represents the shape's area of input arguments. Now suppose that the covariance Σ is very small or near singular, then we enlarge the covariance Σ by a coefficient $\beta \geq 1$ and translate it into the solid red ellipse E_{r2}.

In contrast to ACE, the expanded ellipses are collinear with the original ellipses, i.e., E_{r2} and E_{b2} in TRACE are moved to a new center O_2, which is collinear with the original center O_1 and the coordinate origin O. In doing so, we can simply derive

Algorithm 2: APSE Algorithm for CPP.

Result:
$p(Y < \rho^2)$: future connection probability $p(s_{12}^{k+l} = 1)$;
Data:
$b(\boldsymbol{X}^{k+1:k+L|k}) \sim N(\bar{\boldsymbol{X}}^{k+1:k+L|k}, \boldsymbol{\Sigma})$: propagated belief ;
ρ : ranging maximum of sensors;
δf : desired theoretical limit for the truncation error.
Extract $\boldsymbol{p}_1^{k+l} \sim N(\bar{\boldsymbol{p}}_1^{k+l|k}, \boldsymbol{\Sigma}_1), \boldsymbol{p}_2^{k+l} \sim N(\bar{\boldsymbol{p}}_2^{k+l|k}, \boldsymbol{\Sigma}_2)$, from $b(\boldsymbol{X}^{k+1:k+L|k})$:
Compute $\Delta\boldsymbol{p}_k^{k+1} \sim N(\boldsymbol{\mu}, \boldsymbol{\Sigma})$ by:
  $\boldsymbol{\mu} = \bar{\boldsymbol{p}}_1^{k+1|k} - \bar{\boldsymbol{p}}_2^{k+1|k}, \boldsymbol{\Sigma} = \boldsymbol{\Sigma}_1 + \boldsymbol{\Sigma}_2 - 2\boldsymbol{\Sigma}_{12}$
$[\rho_{3\delta}^{min} \rho_{3\delta}^{max}] \leftarrow 3\delta$ area identification [10] ;
if $\rho < \rho_{3\delta}^{min}$ **then**
  Return $p(Y < \rho^2) = 0$;
else if $\rho > \rho_{3\delta}^{max}$ **then**
  Return $p(Y < \rho^2) = 1$;
end
$[\boldsymbol{\mu}, \boldsymbol{\Sigma}, \rho] \leftarrow$ TRACE$(\boldsymbol{\mu}, \boldsymbol{\Sigma}, \rho)$; /* algorithm 1 */
$\boldsymbol{\lambda} \leftarrow$ compute the eigenvalues of $\boldsymbol{\Sigma}$;
$\boldsymbol{P} \leftarrow$ compute the orthogonal matrix composed of the eigenvectors of $\boldsymbol{\Sigma}$;
$\boldsymbol{b} = P^T\boldsymbol{\Sigma}^{-\frac{1}{2}}\boldsymbol{\mu}$, $y = \rho^2$, $w_m = 50$;
for $r = 0; r \leq w_m; r = r + 1$ **do**
  $d_r \leftarrow$ using (21) for $r = 1, ..., w_m$;
  $c_r \leftarrow$ using (20) by using d_r for $r = 0, ..., w_m$;
  $y_r = (-1)^r \frac{y^{r+1}}{\Gamma(r+2)}, r = 0, ..., k_m$; /* y_r is the right side of (23) without c_r */
  if d_r *reaches its maximum* **then** /* adaptive strategy for selecting w_m */
    $D = d_r$, $w_{m1} = \frac{1}{b_1^2} + \frac{1}{2\lambda_1 - 1}$, $w_{m2} = \frac{1}{b_2^2} + \frac{1}{2\lambda_2 - 1}$,
    $w_{m3} = e^2 y + D$, $w_{m4} = 3D - ln\left(\frac{\delta f}{c_0 y^D}\right) - 1$;
    $w_m = \max(w_{m1}, w_{m2}, w_{m3}, w_{m4}, w_m)$;
  end
end
$F_p(\boldsymbol{\lambda}; \boldsymbol{b}; y) \leftarrow$ (23) using the series c_r, y_r ;
Return $p(Y < \rho^2) = F_p(\boldsymbol{\lambda}; \boldsymbol{b}; \rho)$

the following equation according to basic geometric similarity:

$$\frac{S(\widehat{ABC} \cap E_{r1})}{S(E_{r1})} = \frac{S(\widehat{DEF} \cap E_{r2})}{S(E_{r2})} \tag{54}$$

if $\rho_2 = \sqrt{\beta}\rho_1$.

The pseudocode of TRACE is presented in Algorithm 1. It should be noted that there are various ways to choose a proper expansion coefficient β. In the following algorithm, we calculate β by expanding the covariance matrix to a new one whose smallest eigenvalue is no less than 1. Although TRACE is proposed to deal with the case of a singular or small covariance, we could also revise it inversely by narrowing a larger ellipse at O_2 to a smaller but "well-constructed" one at O_1. This way we can avoid a very large ranging threshold ρ in computation because $y = \rho^2$ is heavily used in our finite-term approximation in (23). A large ρ may also introduce and accumulate

rounding errors from numerical computation on a hardware platform.

D. Adaptive Power Series Expansion (APSE)

So far, we have presented the two main parts of our algorithm. In Section IV-B, we provided a theoretical derivation showing that Theorem 2 can accurately calculate the probability of connection of two nodes as long as the covariance of the relative distance is proper and most importantly that the degree of the finite-term approximation can be adaptively selected. Then in Section IV-C, we provided a novel method for dealing with the constraint of the covariance to extend our method to more general cases. Jointly, we conclude the pseudocode for computing the probability of a future connection in Algorithm 2.

As shown by the top-down order, this algorithm takes as inputs the estimated mean $\boldsymbol{\mu}$, covariance $\boldsymbol{\Sigma}$ of the relative distance distribution of two nodes, and the ranging threshold ρ. It finally returns the probability of the event $Y = d_{12}^2 < \rho^2$. Lines 4–8 are the content of 3δ regulation, which has been developed and explained in our previous work [10]. The purpose of preserving this part is to reduce the computational complexity when the relative distance computed from the estimated means lies far beyond the 99.7% sample coverage area (i.e., 3δ area). So we just simply assign the probability to be 1 or 0 and accept the consequently possible 0.03% error.

Moving on, the TRACE algorithm is called in line 10 to derive a proper covariance $\boldsymbol{\Sigma}$ whose eigenvalues meet the critical constraint in (35). Meanwhile, the mean vector $\boldsymbol{\mu}$ and ranging threshold ρ would be updated accordingly. Then lines $11-22$ are the computation of our proposed finite-term approximation of Theorem 2. Within the pseudocode, we first give an initial value of the selected degree $w_m = 50$ so that we can find the maximum of the series d_w. Note that the initialization of w_m presented here is not necessary but is instrumental in the preallocation of storage. Here, we suppose that d_w can reach its peak within the first 50 elements and therefore our code could enter lines 18–21. Here are the main results of Theorem 1 for adaptively choosing a proper degree w_m for the summation. We note that this part only needs to be run once and since we compare all the candidates of w_m with the initial at line 20 the total number of summations of our finite-term approximation in (23) will be at least 50.

Algorithm 3: Bernoulli Model.

Result: $p(Y < \rho^2)$
Data: $\boldsymbol{\mu}$, ρ ;
1 $Pr(Y < \rho^2) = 0$; /* Initialized with 0 */
2 **if** $||\boldsymbol{\mu}||_2 \leq \rho$ **then**
3 $p(Y < \rho^2) = 1$
4 **end**
5 **Return** $p(Y < \rho^2)$

Algorithm 4: Linear Model.

Result: $p(Y < \rho^2)$
Data: $\boldsymbol{\mu}$, $\boldsymbol{\Sigma}$, ρ ;
1 $[\rho_{3\delta}^{min}, \rho_{3\delta}^{max}] \leftarrow 3\delta$ area identification;
2 **if** $\rho \leq \rho_{3\delta}^{min}$ **then**
3 **Return** $Pr(Y < \rho^2) = 1$
4 **else if** $\rho > \rho_{3\delta}^{min}$ **then**
5 **Return** $Pr(Y < \rho^2) = 0$
6 **end**
7 **Return** $p(Y < \rho^2) = \frac{1}{\rho_{3\delta}^{max} - \rho_{3\delta}^{min}} (\rho - \rho_{3\delta}^{min})$;

Algorithm 5: Random Sampling-Based Model.

Result: $p(Y < \rho^2)$
Data: $\boldsymbol{\mu}, \boldsymbol{\Sigma}, \rho, dim$;
1 Count = 0 ;
2 **while** $k \leq dim$ **do**
3 data $\leftarrow$ RandomlySample($\boldsymbol{\mu}, \boldsymbol{\Sigma}$) ;
4 **if** $||data||_2 \leq \rho$ **then**
5 Count = Count + 1 ;
6 **end**
7 **end**
8 **Return** $p(Y < \rho^2) = \frac{Count}{dim}$;

V. Simulations and Results

In this section, we present extensive analyses of the proposed methods and perform comparisons against benchmark methods from related works. We first evaluate the performance of APSE in Algorithm 2 in terms of accuracy and computational efficiency. Then, two instances of the *cooperative localization and active planning* (CLAP) problem are investigated. The first is drawn from our prior work [10] and formulates the problem as a one-step finite state MDP (OS-MDP), where the state space consists of all possible network topologies and the reward is a function of the leader's localization uncertainty. The second is derived from a patrolling task and we study the impact of a longer planning horizon by using a generalized belief space formulation (GBS).

In addition, to show the effectiveness of the proposed APSE algorithm in active planning problems, we compare against several prevailing approaches that solve the CPP in existing works, these are

1) a deterministic *Bernoulli* model in Algorithm 3.
2) a *Linear* distribution in Algorithm 4.
3) a *Random* sampling-based distribution in Algorithm 5.

Note that the Bernoulli distribution has been widely applied to many existing active planing problems by taking the well known ML assumption [5]. This is due to the similarity it offers to the estimation problem, whereby the standard estimation engines (for both the filtering method and smoothing formulation) can be directly introduced to recover the future beliefs given a control candidate. As a result the corresponding cost can be easily derived. The linear distribution, however, is a partly empirical formula, which does not consider the exact motion and measurement models. Indelman et al. [6] came up with this method in their problem formulation to show the influence of uncertain observations but no further detail is given about how the active

planning framework can deal with such a probabilistic future measurement and communication topology. Finally, the random sample distribution is a completely intuitive method, which uses the frequency of a connection to represent its probability as used in [7]. However, the number of samples may lead to different performance in terms of predictive precision and computational tractability.

The code for all simulations was implemented in Matlab R2019a and executed on a Windows machine with an i7-9750H @ 2.6 GHz processor and 8 GB of memory.

A. Performance of APSE

In this section, we test our proposed APSE in Algorithm 2 to evaluate its probability accuracy and computational complexity. By comparing against existing methods, we will show that one great advantage of APSE is its high precision. Since the Bernoulli and linear models are merely two rough guesses of the real distribution of the connection, we only compare our proposed algorithm against the random sampling-based method with different sampling degrees.

Before moving on, we remark here that the implementation of our proposed probability algorithm is realized using the for-loop in MATLAB, while the comparison methods using random sampling apply the built-in function `mvrnd`. Therefore, the computation time performance of our proposed APSE algorithm, presented in this subsection, could be further improved if more optimization can be introduced.

The setup is given as follows. We test two nodes A and B whose estimated means are fixed to $\boldsymbol{p}_A = [0.5, 1]^T$ and $\boldsymbol{p}_B = [2, 2.5]^T$ and the mean distance between them is $||\boldsymbol{p}_A - \boldsymbol{p}_B||_2 \approx 2.21$. In each simulation trial, we do the following actions:

1) Randomly generate two symmetric and positive matrices $\boldsymbol{P}_A > 0, \boldsymbol{P}_B > 0$ as the covariance of nodes A and B.

2) *Experimental method:* for each range ρ in the sets $\boldsymbol{S}_\rho := \{0.1 : 0.1 : 6\}$, $\boldsymbol{p}_A, \boldsymbol{p}_B, \boldsymbol{P}_A, \boldsymbol{P}_B$, and ρ are taken as the input of APSE with the desired accuracy $\delta f = 10^{-10}$. We record the output probability and run time corresponding to each $\rho \in \boldsymbol{S}_\rho$ into the set $\boldsymbol{P}_{APSE}$ and $\boldsymbol{T}_{APSE}$, whose sizes are both 60.

3) *Comparison methods:* Random sampling (Algorithm 5) is tested for six different sampling degrees, i.e., dim $= [10, 10^2, 10^3, 10^4, 10^5, 10^6, 10^7]$. For each dim, repeat step 2) and record six sets of probabilities $\boldsymbol{P}_{dim}$ and run times $\boldsymbol{T}_{dim}$. When dim $= 10^7$, the probability is treated as the ground truth, i.e., $\boldsymbol{P}_{dim=10^7} = \boldsymbol{P}_{truth}$.

4) Compute the root mean squared error (RMSE) for each method in $\{APSE, 10, 10^2, 10^3, 10^4, 10^5, 10^6, 10^7\}$:

$$RMSE_{method} = \sqrt{\sum_{i=1}^{60} [\boldsymbol{P}_{method}(i) - \boldsymbol{P}_{truth}(i)]^2}$$

and compute the mean run time per calculation as

$$MeanRunTime = \frac{1}{60} \sum_{i=1}^{60} (\boldsymbol{T}_{method}(i)).$$

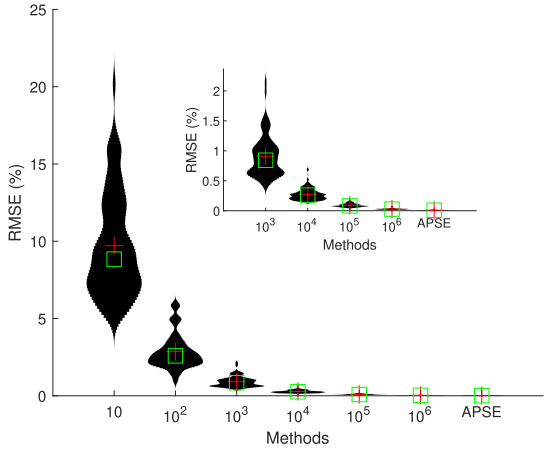

Fig. 3. RMSE distribution over 200 trials.

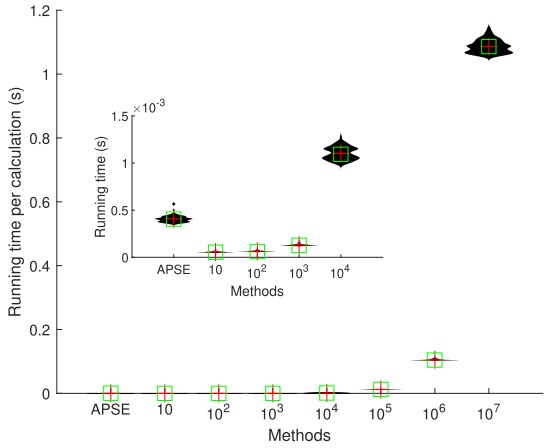

Fig. 4. Mean run time distribution over 200 trials.

The statistical distribution of both RMSE and mean run time per calculation over 200 trials are presented in Figs. 3 and 4, respectively. It is not surprising to see that the comparison group, the random sampling-based algorithm, produces higher calculation accuracy but worse computational complexity as the sampling degree gets larger. The experimental group, the APSE Algorithm 2, surpasses all the comparison groups in terms of probability precision, which is indicated by RMSE. At the same time, it achieves a relatively moderate computational complexity, remaining in the same order of magnitude as the random sampling algorithm with degree between 10^3 and 10^4.

B. CLAP With OS-MDP

As depicted in Fig. 5, this simulation follows a similar setup to our previous work [10]. Here we consider a MRS consisting of one leader and four followers in a GNSS-limited and noisy environment. All robots only know their initial positions exactly (as shown in Table III) and need to localize themselves due to the existence of motion noise. A point-mass motion model corrupted with Gaussian noise is considered

$$\boldsymbol{p}_i^{k+1} = \boldsymbol{p}_i^k + \boldsymbol{u}_i^k + \boldsymbol{w}_i$$

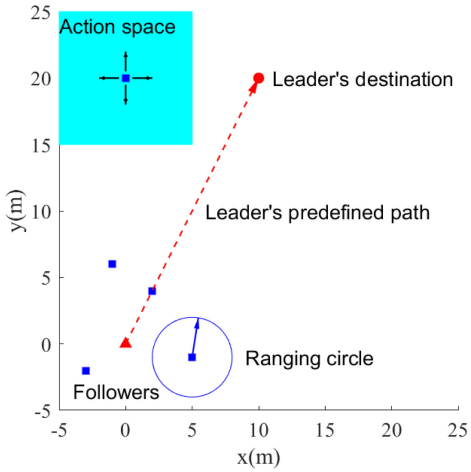

Fig. 5. Initial configuration of the CLAP problem with an OS-MDP active planning framework.

TABLE III
INITIAL POSITIONS FOR THE LEADER AND FOUR FOLLOWERS

Nodes	L	F1	F2	F3	F4
Pos(m)	[0;0]	[-1;6]	[2;4]	[5;-1]	[-3;-2]

where $\boldsymbol{w}_i \sim \mathcal{N}(\boldsymbol{0}, \boldsymbol{R}), \forall i \in \mathcal{V}$ with known information matrix $\boldsymbol{R} = \text{diag}([0.04, 0.04])$. The leader is initially located at the bottom-left corner and is tasked to reach its destination by traversing the mission plane along a predefined trajectory. The leader's motion strategy used in this simulation is calculated simply by heading toward the destination, i.e.,

$$\boldsymbol{u}_L = u_{max} \frac{\boldsymbol{p}_{des} - \hat{\boldsymbol{p}}}{||\boldsymbol{p}_{des} - \hat{\boldsymbol{p}}||_2}$$

where $\boldsymbol{p}_{des}$ is the position of the destination, $\hat{\boldsymbol{p}}$ is the estimated position of the leader, and u_{max} is the limited moving distance at each time step.

Four followers are deployed to help reduce the leader's accumulated localization uncertainty during the mission by optimizing their motion sequences. The action space for each follower is set as

$$\boldsymbol{A}_i = [0;1], [1;0], [0;-1], [-1;0].$$

All robots equip ranging devices whose maximum measurement distance is set $\rho = 3\,m$. As no global localization is available in the mission space and no landmarks or anchors are available, the relative measurements between robots are the only information source for robots to correct their localization uncertainty. The measurement model used in the simulation is exactly (5) with known information matrix $Q = 0.01$ and the active planning framework is the OS-MDP [10] with a one-step-ahead planning horizon. The immediate cost is computed as the leader's localization uncertainty

$$c^l\left(b\left(\boldsymbol{x}^{k+1,\boldsymbol{U}^k}\right)\right) = \text{trace}\left(\boldsymbol{\Sigma}_{\boldsymbol{p}_L^{k+1}}\right).$$

All four methods of predicting the probability of future connectivity are tested for 50 trials and the statistical results are

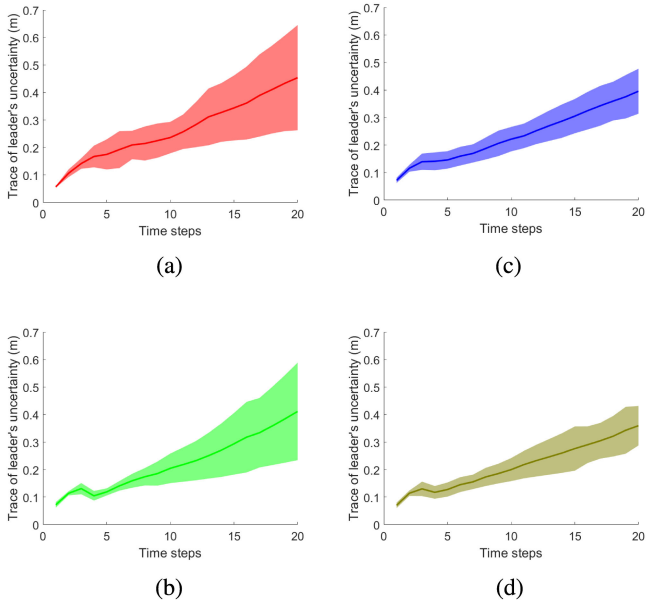

Fig. 6. (a)–(d) Statistical distribution of the leader's localization uncertainty over 50 trials for CLAP with OS-MDP.

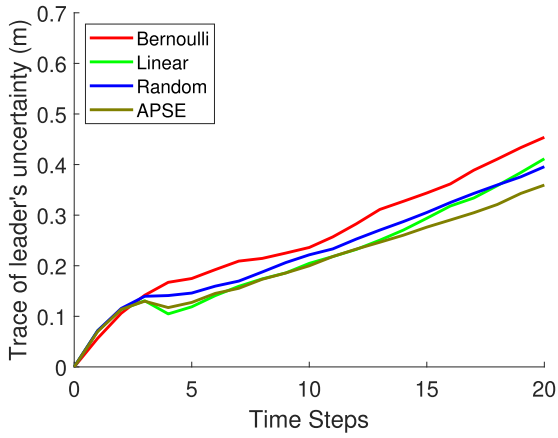

Fig. 7. Leader's mean uncertainties over 50 trials for all four methods.

TABLE IV
FINAL TRACE OF THE LEADER'S LOCALIZATION COVARIANCE

Methods	Mean ± std (m)	APSE improvement
Bernoulli	0.4539 ± 0.1914	20.8%
Linear	0.4114 ± 0.1774	12.6%
Random	0.3958 ± 0.0818	9.2 %
APSE	**0.3595 ± 0.0719**	–

shown in Figs 6 and 7. Besides, the mean and standard deviation of the trace of leader's localization covariance at the final step are also calculated and listed in Table IV.

It is not surprising to see that the distributions of the trace for all four methods all keep increasing and diverging. There is no fixed location source and therefore the absolute drift of the overall system cannot be corrected. More theoretical results of this observation can be found in [31]. However, we also observe that our proposed APSE algorithm surpasses all the existing

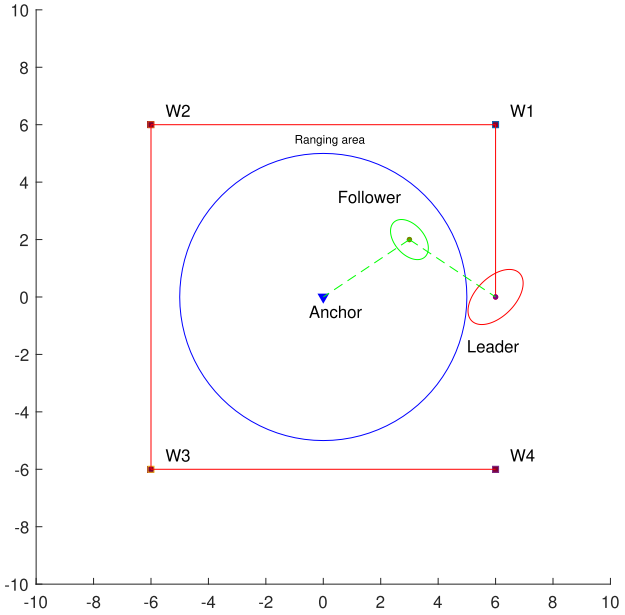

Fig. 8. Initial configurations of the CLAP problem.

methods, i.e., {Bernoulli, Linear, and Random}. Our proposed APSE algorithm has the slowest localization performance decay and improves over the other methods by {20.8%, 12.6%, 9.2%}, respectively. Therefore, we conclude that a more accurate probability of future connection can indeed help improve the performance of active planning in noisy environments.

C. CLAP With Generalized Belief Space (GBS)

We investigate a more realistic MRS planning scenario based on a patrolling mission and allow a longer planning horizon. Here, two mobile robots operate in a noisy and GNSS-limited environment, of which robot L is the leader robot responsible for the high-level tasks that are assigned by a human operator. The follower robot F is scheduled to help the leader reduce its localization uncertainty. The follower serves as a relay node that actively and optimally generates extra communication and observation links when the leader is out of the anchor's coverage area. The single anchor in the scene knows its exact position and can communicate with and observe nodes within its coverage area. The initial configuration is illustrated in Fig. 8, where the leader is executing a cruise or monitoring mission whose predefined trajectory is completely out of the communication and observation range of the anchor. Through a relay node, the leader is virtually connected to the anchor by the relay link as demonstrated by the green dashed lines in Fig. 8. The quality of such a virtual connection depends on the relative position of the measurement graph, which can be controlled by optimizing the follower's trajectory.

The motion and measurement models applied in this scenario are the same as the previous simulation experiment. The planning horizon is set to 3 s look-ahead. Denoting $\tilde{\boldsymbol{p}}_L^l$ and $\boldsymbol{\Sigma}_{\tilde{\boldsymbol{p}}_L^l}$ as the predicted mean and covariance of the leader robot while $\tilde{\boldsymbol{p}}_F^l$ and $\boldsymbol{\Sigma}_{\tilde{\boldsymbol{p}}_F^l}$ as those of the follower, then the immediate cost in the objective function is defined as

$$c^l\left(b\left(\boldsymbol{X}^{k+l}, \boldsymbol{U}^{k+l-1}\right)\right) = \omega_1 trace\left(\boldsymbol{\Sigma}_{\tilde{\boldsymbol{p}}_L^l}\right) + \omega_2 trace\left(\boldsymbol{\Sigma}_{\tilde{\boldsymbol{p}}_F^l}\right). \tag{55}$$

The initial positions are $\boldsymbol{p}_L^0 = [6, 0]^T$ and $\boldsymbol{p}_F^0 = [3, 2]^T$. The anchor is located at the origin. Initially there is a connection between the follower and anchor. Both robots are initialized with some localization uncertainty. The leader's high-level trajectory is defined by four sequential waypoints $W_1 = [6, 6]^T, W_2 = [-6, 6]^T$, $W_3 = [-6, -6]^T, W_4 = [6, -6]^T$. We calculate the leader's control input by directly heading to its destination waypoint, which switches to next one once $d_{L\to W_j} = ||\bar{\boldsymbol{p}}_L - W_j|| < 0.2\,m$, where $\bar{\boldsymbol{p}}_L$ is the leader's estimated position. The maximum moving distance at each time step for leader and follower are 0.5 m and 0.7 m, respectively. The gains in the objective function are chosen as $\omega_1 = 9$ and $\omega_2 = 1$. The GBS proposed in [6] is utilized as the active planning framework.

Statistical results are presented in Fig. 9(a)–(d) showing the distribution of the leader's localization uncertainty over 20 trials. Notice that the total run time for every trial differs since different control strategies are executed due to varying localization uncertainties. The lighter vertical bars in each distribution show the time ranges when the leader reaches each waypoint. The horizontal colored bar along the top demonstrates the number of active trials at the corresponding time step.

We further collect the processed characteristics for all four methods into one plot to make a clearer comparison as shown in Fig. 9(e) and (f). Here two performance metrics are considered, the evolution of the trace of the leader's uncertainty and the mean RMSE of the leader's localization error (deviation between the estimated and real position). More statistical results are computed and compared in Table V. The performance metrics considered here are as follows:

1) mm-RMSE: the leader's localization RMSE when taking the mean over all time steps and over all trials.

2) mm-Trace: trace of the leader's covariance matrix when taking the mean over all time steps and over all trials.

3) m-TotalCon: mean over 20 trials of the total number of the relay connections transmitting location information from anchor to leader through follower in each trial.

4) m-TotalTra: mean distance of the leader's real trajectory for each trial. The distance of the nominal trajectory assuming perfect knowledge of the leader's position is 42 m.

By comparing Fig. 9(e) and (f), we can draw two main conclusions:

1) the methods {Linear, Random, APSE} under probabilistic connection perform better than the traditional approach, Bernoulli, under a deterministic connection;

2) the localization uncertainty becomes more convergent and its mean uncertainty is smaller if a more accurate algorithm, such as APSE, is used to calculate the connection probability.

From Table V, an evident conclusion that can be directly derived is that our proposed APSE method surpasses all other approaches {Bernoulli, Linear, Random}. The improvement in performance of mm-RMSE for APSE is {24.28%, 22.18%,

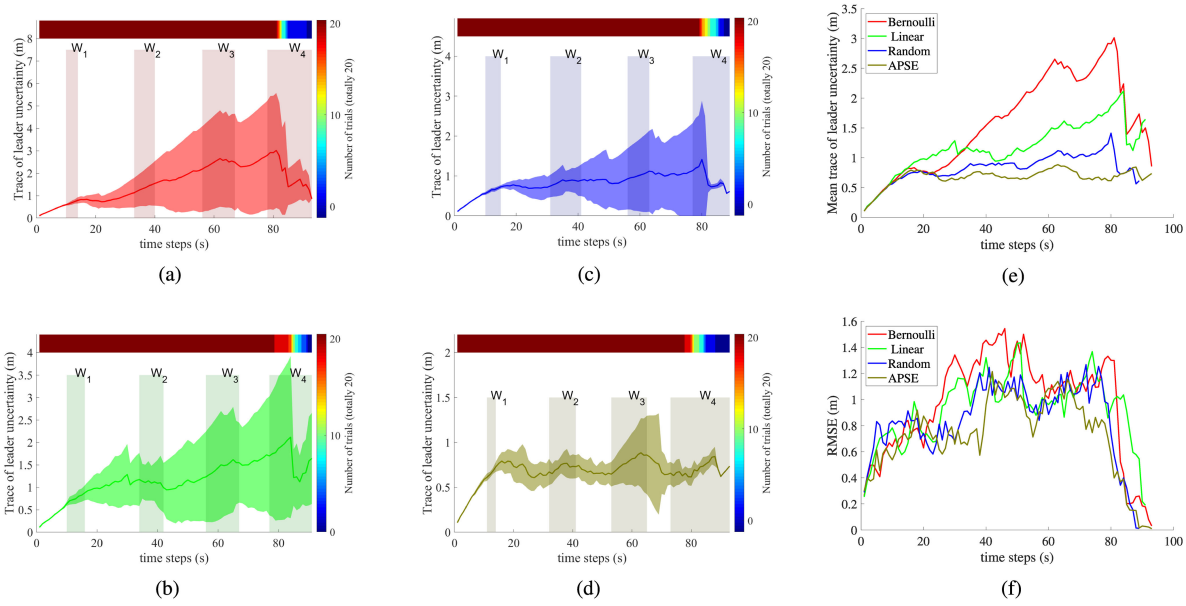

Fig. 9. (a)–(d) Statistical distribution of the leader's localization uncertainty over 20 trials for CLAP with GBS. The vertical shaded bars marked by W_1–W_4 indicate the distribution of times that leader reaches that waypoint. The colormap shows how many trials exist across the time line. Note that they have different scales on their axes. (e) Leader's mean localization uncertainty for four methods in one figure. (f) Mean RMSE of the leader's localization deviation.

TABLE V
STATISTICAL CHARACTERISTICS OVER 20 TRIALS

Performance metrics	Methods			
	Bernoulli	Linear	Random	APSE
mm-RMSE (m)	1.0669	1.0381	0.9119	**0.8079**
mm-Trace (m)	1.5651	1.1715	0.8208	**0.6752**
m-TotalCon	41.85 ± 23.47	44.70 ± 14.09	66.85 ± 20.07	**75.85 ± 8.85**
m-TotalTra (m)	47.1090 ± 1.9839	46.9427 ± 2.4161	46.6451 ± 1.6078	**45.7925 ± 1.5493**

11.40%} when compared with the other three methods. As for the mm-Trace, its reduction rates are respectively {56.86%, 42.36%, 17.74%}. In addition, the comparative increase in the m-TotalCon is {81.24%, 75.73%, 13.47%}.

Regarding the traveled distance, a more meaningful way is to compare the extra distance, computed by subtracting the nominal shortest trajectory from the executed one. Intuitively, the extra travel distance is introduced due to the existence of uncertainties and hence it can reflect how uncertainties are accumulated across the evolution. As the leader's nominal travel distance is 42 m, we say that by applying the underlying four active planning strategies, the extra distances are {5.1090, 4.9427, 4.6451, 3.7925}m. Therefore, our proposed APSE achieves a {25.76%, 23.27%, 18.35%} reduction on the distance traveled.

VI. CONCLUSION AND FUTURE WORKS

This note addressed the algorithmic challenges in active planning problems that arise when the future observation/communication connection is unknown at the time of planning. The most important contribution is an improved algorithm—APSE—for computing the exact probability of a future connection considering the disk communication and observation model based on available information at the current time and given the control candidates. Through both theoretical analyses and numerical simulations, three conclusions are made as follows:

1) The APSE can achieve a theoretically guaranteed accuracy under an adaptive selection of the summation degree.

2) The computational complexity of APSE is at the same magnitude as random sampling methods with their number of samples between 10^3 and 10^4.

3) We have verified the idea that the performance of active planning can indeed be further improved by accurately predicting the distribution of future unknown variables.

However, despite the aforementioned achievements, the APSE algorithm still suffers from round-off error from the computation platform. This error may significantly impact its accuracy if the communication and observation threshold ρ is too large. Though the TRACE algorithm can be used inversely to deal with this problem, the critical requirement on the eigenvalues of the covariance still restricts its performance. A direct way to address this problem is by applying packages with higher precision of quantities such as the Multiple Precision Toolbox for the MATLAB platform https://www.advanpix.com/. Another roadmap may refer to the variants of a standard chi-square distribution, where a look-up table is often used to search for the probability and interpolation needed for the values missing in the table. Either Patnaik's approximation [47] or Pearson's approximation [48] may be an underlying solution.

In addition, more investigations should be conducted to reason about the independence relationships depicted in (14) and (15) regarding future connectivities. Though spatial independence can be established by the separated measurement process, temporal independence should be further looked into, especially in terms of the applicability of the Markov assumption.

Moving on, another important topic is to extend our analysis from 3 DOF to 6 DOF. The key challenge in such an extension is how to build a mathematical measurement model and reason about the correlation between the limits of the measurement model caused by future positions and attitudes.

Finally, more complex environments could be taken into further consideration. Here we only assume an empty world with an ideal disk communication and observation model. However, real deployment of the active planning problem will likely have to deal with different configurations, like physical obstructions in the environment, the blocking of data transmission or radio measurement signals, the separation of communication and observation devices, various types of sensor noise, faults, failures, etc.

APPENDIX A

Recalling the definition of the coefficient d_w (21), we know the subtraction of two consecutive terms, d_{w+1} and d_w is

$$d_{w+1} - d_w = \frac{(2\lambda_j)^{-w}}{2} \sum_{j=1}^{2} \left\{ w b_j^2 \left[1-(2\lambda_j)^{-1}\right] + \left(1-b_j^2\right)(2\lambda_j)^{-1} - 1 \right\}. \tag{56}$$

As we have $[1-(2\lambda_j)^{-1}] > 0$, then if

$$w \geq \frac{1}{b_j^2} + \frac{1}{2\lambda_j - 1} \qquad \forall j \in \{1,2\} \tag{57}$$

the subtraction has

$$d_{w+1} - d_w > 0.$$

Moreover, it is clear that $d_w \leq 0, \forall w \in \mathbb{N}^+$ if

$$w \geq \frac{1}{b_j^2} \quad \forall j \in \{1,2\}. \tag{58}$$

From (21), the limit of d_w is

$$\lim_{w\to\infty} d_w = \lim_{k\to\infty} \sum_{j=1}^{p} \left(\frac{1}{(2\lambda_j)^w} - b_j^2 \frac{w}{(2\lambda_j)^w} \right) \quad \forall j \in 1,2.$$

Then according to the well-known L'Hopital rule, if $2\lambda_j > 1$, the right-hand side of the limit is exactly zero.

In conclusion, we derive that if the given distribution of relative distance between two nodes is well-defined, i.e., $\lambda > \frac{1}{2}$, the output of $|d_w|$ will keep decreasing when the degree w grows large enough to realize the conditions in (57), as the condition in (58) is included in (57). Therefore, we know that there exists a maximum $d^u > 0$ so that $|d_w| < d^u, \forall w \in \mathbb{R}^+$.

This ends the proof of Corollary 1.

APPENDIX B

Let expand two consecutive terms $\tilde{c}_{w+1}$ and $\tilde{c}_w$,

$$w\tilde{c}_w = \left(\tilde{c}_0 \tilde{d}_w + \tilde{c}_1 \tilde{d}_{w-1} + \cdots + \tilde{c}_{w-1} \tilde{d}_1 \right) \tag{59}$$

and

$$(w+1)\tilde{c}_{w+1} = \left(\tilde{c}_0 \tilde{d}_{w+1} + \tilde{c}_1 \tilde{d}_w + \cdots + \tilde{c}_w \tilde{d}_1 \right). \tag{60}$$

Adding $\tilde{c}_w$ to both sides of (59) derives

$$(w+1)\tilde{c}_w = \left(\tilde{c}_0 \tilde{d}_w + \tilde{c}_1 \tilde{d}_{w-1} + \cdots + \tilde{c}_{w-1} \tilde{d}_1 + \tilde{c}_w \right). \tag{61}$$

Taking the subtraction of (61) and (60) has

$$\begin{aligned} &(w+1)\left(\tilde{c}_{w+1} - \tilde{c}_w\right) \\ &= \tilde{c}_0 \left(\tilde{d}_{w+1} - \tilde{d}_w \right) + \cdots + \tilde{c}_{w-1} \left(\tilde{d}_2 - \tilde{d}_1 \right) + \tilde{c}_w \left(\tilde{d}_1 - 1 \right). \end{aligned} \tag{62}$$

Since $\tilde{d}_{w+1} = \tilde{d}_w = \ldots = \tilde{d}_1 = d^u$, we can further get

$$\begin{aligned} &(w+1)\left(\tilde{c}_{w+1} - \tilde{c}_w\right) = \left(d^u - 1\right)\tilde{c}_w \\ \Rightarrow \quad &\tilde{c}_{w+1} = \frac{d^u + w}{w+1} \tilde{c}_w. \end{aligned} \tag{63}$$

Recalling that $\tilde{c}_0 = c_0 > 0$, then we know $\tilde{c}_w > 0, \forall w \in \mathbb{N}^+$.

Next, we need to show that $|c_w| \leq |\tilde{c}_w|, \forall w \in \mathbb{N}^+$. It has been already shown that $c_0 = \tilde{c}_0 \Rightarrow |c_0| \leq |\tilde{c}_0|$. Hence, we have

$$|c_1| = |c_0 d_1| \leq |c_0||d^u| = |\tilde{c}_1|. \tag{64}$$

Similarly, we suppose that $|c_i| \leq |\tilde{c}_i|$ when $i = w-1$. Then we can derive

$$\begin{aligned} |c_w| &= \left| \frac{1}{w} \left(c_0 d_w + c_1 d_{w-1} + \cdots + c_{w-1} d_1 \right) \right| \\ &\leq \frac{1}{w} \left(|\tilde{c}_0||d^u| + |\tilde{c}_1||d^u| + \cdots + |\tilde{c}_{w-1}||d^u| \right) = |\tilde{c}_w|. \end{aligned} \tag{65}$$

Note that the above equation is held by the fact that two new series $\tilde{c}_w$ and $\tilde{d}_w$ are all positive.

Similarly, we can also conclude the same result as shown above when $i > w-1$. Therefore, the conclusion in (31) can be drawn. This ends the proof of Corollary 2.

APPENDIX C

A similar series $\tilde{e}_w^D$ can be built using $\tilde{c}_w$ according to the definition of e_w^D in (32) and (33). Therefore, the relationship between c_w and $\tilde{c}_w$ in (31) can be equally extended to e_w^D and $\tilde{e}_w^D$, whereby we know that

$$|e_w^D| \leq |\tilde{e}_w^D| \quad \forall w \in \mathbb{N}^+.$$

According to (30), the following extension can be made when $w \geq D-1$:

$$\tilde{e}_{w+1}^D = \frac{d^u + w}{w+1} \frac{\prod_{j=1}^{D}(w+2-j)}{\prod_{j=1}^{D}(w+3-j)} \tilde{e}_w^D. \tag{66}$$

So, if $D = 1$, we derive,

$$\tilde{e}^1_{w+1} = \frac{d^u + w}{w+2}\tilde{e}^1_w < \tilde{e}^1_w \quad \forall w \geq 0. \tag{67}$$

This means $\tilde{e}^1_w$ gets smaller when w tends to infinity.

Otherwise, when D is general and $D \geq 2$, we have

$$\begin{aligned}\tilde{e}^D_{w+1} &= \frac{d^u + w}{w+1}\frac{(w+1)(w+2-D)\prod_{j=2}^{D-1}(w+2-j)}{(w+2)(w+1)\prod_{j=3}^{D}(w+3-j)}\tilde{e}^D_w \\ &\leq \frac{(d^u + w)(w+2-D)}{(w+2)(w+1)}\frac{\prod_{j=2}^{D-1}(w+2-j)}{\prod_{j=2}^{D-1}(w+2-j)}\tilde{e}^D_w \\ &= \frac{(d^u + w)(w+2-D)}{(w+2)(w+1)}\tilde{e}^D_w \quad \forall w \geq D-1.\end{aligned} \tag{68}$$

A simple calculation derives

$$\begin{aligned}&(d^u + w)(w+2-D) - (w+2)(w+1) \\ &= (d^u - D - 1)w + d^u(2-D) - 2.\end{aligned}$$

As we know that $0 \leq d^u \leq D$ and $D \geq 2$, hence $(d^u - D - 1) < 0$ and $d^u(2-D) - 2 < 0$. As a result, $\tilde{e}^D_w$ is also decreasing when $w \geq D-1$, i.e., $\tilde{e}^D_{w+1} < \tilde{e}^D_w, \quad \forall w \geq D-1$. Therefore, the limit of $\tilde{e}^D_k$ is bounded, $\lim_{w\to\infty}\tilde{e}^D_w = \text{Const}$.

Since $\tilde{e}^D_w$ is the envelope of e^D_w, then the limit of $|e^D_w|$ is also bounded, which gives the result in (34). The maximum of $\tilde{e}^1_w$ is obviously the first element $e^1_0 = \tilde{c}_0$. As for $D \geq 2$, we recall the relationship of $\tilde{c}_w$ and $\tilde{c}_{w+1}$ in (30). We know that $\tilde{e}^D_w$ is increasing when $w \leq D-2$ and the last element $\tilde{e}^D_{D-2} = \tilde{c}_{D-2}$ is the largest value thus far. After that, $\tilde{e}^D_w$ will decrease over the increment of w, which gives its peak value $\tilde{e}^D_{D-1} = \frac{\tilde{c}_{D-1}}{D!} \leq \tilde{c}_{D-1}$ when $w \geq D-1$. Since we have $\tilde{c}_{D-2} < \tilde{c}_{D-1}$, the maximum value of $\tilde{e}^D_w$ is therefore $\tilde{c}_{D-1}$. Consequently, it is also the upper boundary of $|e^D_w|$. This ends the proof of Corollary 3.

REFERENCES

[1] C. Cadena et al., "Past, present, and future of simultaneous localization and mapping: Toward the robust-perception age," *IEEE Trans. Robot.*, vol. 32, no. 6, pp. 1309–1332, Dec. 2016.

[2] Y. S. Hidaka, A. I. Mourikis, and S. I. Roumeliotis, "Optimal formations for cooperative localization of mobile robots," in *Proc. IEEE Int. Conf. Robot. Automat.*, 2005, pp. 4126–4131.

[3] B. Schlotfeldt, D. Thakur, N. Atanasov, V. Kumar, and G. J. Pappas, "Anytime planning for decentralized multirobot active information gathering," *IEEE Robot. Automat. Lett.*, vol. 3, no. 2, pp. 1025–1032, Apr. 2018.

[4] N. Patwari, J. N. Ash, S. Kyperountas, A. O. Hero, R. L. Moses, and N. S. Correal, "Locating the nodes: Cooperative localization in wireless sensor networks," *IEEE Signal Process. Mag.*, vol. 22, no. 4, pp. 54–69, Aug. 2005.

[5] R. Platt, R. Tedrake, L. Kaelbling, and T. Lozano-Perez, "Belief space planning assuming maximum likelihood observations," in *Proc. Robot., Sci. Syst.*, Zaragoza, Spain, 2010. [Online]. Available: http://www.roboticsproceedings.org/rss06/p37.html

[6] V. Indelman, L. Carlone, and F. Dellaert, "Planning in the continuous domain: A generalized belief space approach for autonomous navigation in unknown environments," *Int. J. Robot. Res.*, vol. 34, no. 7, pp. 849–882, 2015.

[7] S. Pathak, A. Thomas, and V. Indelman, "A unified framework for data association aware robust belief space planning and perception," *Int. J. Robot. Res.*, vol. 37, no. 2–3, pp. 287–315, 2018.

[8] E. I. Farhi and V. Indelman, "IX-BSP: Belief space planning through incremental expectation," in *Proc. Int. Conf. Robot. Automat.*, 2019, pp. 7180–7186.

[9] V. Indelman, "Cooperative multi-robot belief space planning for autonomous navigation in unknown environments," *Auton. Robots*, vol. 42, no. 2, pp. 353–373, 2018.

[10] L. Zhang, Z. Zhang, R. Siegwart, and J. J. Chung, "A connectivity-prediction algorithm and its application in active cooperative localization for multi-robot systems," in *Proc. IEEE Int. Conf. Robot. Automat.*, 2020, pp. 9824–9830.

[11] A. Mathai and S. B. Provost, *Quadratic Forms in Random Variables: Theory and Applications*. New York, NY, USA: Marcel Dekker, Inc., 1992.

[12] M. L. Puterman, *Markov Decision Processes: Discrete Stochastic Dynamic Programming*. Hoboken, NJ, USA: Wiley, 2014.

[13] E. V. Denardo, *Dynamic Programming: Models and Applications*. Chelmsford, MA, USA: Courier Corporation, 2012.

[14] G. Shani, J. Pineau, and R. Kaplow, "A survey of point-based POMDP solvers," *Auton. Agents Multi-Agent Syst.*, vol. 27, no. 1, pp. 1–51, 2013.

[15] D. Hsu, Wee Sun Lee, and N. Rong, "A point-based POMDP planner for target tracking," in *Proc. IEEE Int. Conf. Robot. Automat.*, 2008, pp. 2644–2650.

[16] J. Wang, X. Li, and M. Q.-H. Meng, "An improved RRT algorithm incorporating obstacle boundary information," in *Proc. IEEE Int. Conf. Robot. Biomimetics*, 2016, pp. 625–630.

[17] S. Prentice and N. Roy, "The belief roadmap: Efficient planning in belief space by factoring the covariance," *Int. J. Robot. Res.*, vol. 28, no. 11–12, pp. 1448–1465, 2009.

[18] A.-A. Agha-Mohammadi, S. Chakravorty, and N. M. Amato, "Firm: Sampling-based feedback motion-planning under motion uncertainty and imperfect measurements," *Int. J. Robot. Res.*, vol. 33, no. 2, pp. 268–304, 2014.

[19] D. Kopitkov and V. Indelman, "No belief propagation required: Belief space planning in high-dimensional state spaces via factor graphs, the matrix determinant lemma, and re-use of calculation," *Int. J. Robot. Res.*, vol. 36, no. 10, pp. 1088–1130, 2017.

[20] D. Kopitkov and V. Indelman, "General-purpose incremental covariance update and efficient belief space planning via a factor-graph propagation action tree," *Int. J. Robot. Res.*, vol. 38, no. 14, pp. 1644–1673, 2019.

[21] M. A. Hsieh, A. Cowley, V. Kumar, and C. J. Taylor, "Maintaining network connectivity and performance in robot teams," *J. Field Robot.*, vol. 25, no. 1–2, pp. 111–131, 2008.

[22] M. Fiedler, "Algebraic connectivity of graphs," *Czechoslovak Math. J.*, vol. 23, no. 2, pp. 298–305, 1973.

[23] Y. Kim and M. Mesbahi, "On maximizing the second smallest eigenvalue of a state-dependent graph Laplacian," in *Proc. Amer. Control Conf.*, 2005, pp. 99–103.

[24] P. Yang, R. A. Freeman, G. J. Gordon, K. M. Lynch, S. S. Srinivasa, and R. Sukthankar, "Decentralized estimation and control of graph connectivity for mobile sensor networks," *Automatica*, vol. 46, no. 2, pp. 390–396, 2010.

[25] M. Franceschelli, A. Gasparri, A. Giua, and C. Seatzu, "Decentralized estimation of Laplacian eigenvalues in multi-agent systems," *Automatica*, vol. 49, no. 4, pp. 1031–1036, 2013.

[26] M. M. Zavlanos and G. J. Pappas, "Potential fields for maintaining connectivity of mobile networks," *IEEE Trans. Robot.*, vol. 23, no. 4, pp. 812–816, Aug. 2007.

[27] M. M. Zavlanos, M. B. Egerstedt, and G. J. Pappas, "Graph-theoretic connectivity control of mobile robot networks," in *Proc. IEEE Proc. IRE*, vol. 99, no. 9, pp. 1525–1540, Sep. 2011.

[28] Y. Kantaros and M. M. Zavlanos, "Distributed intermittent connectivity control of mobile robot networks," *IEEE Trans. Autom. Control*, vol. 62, no. 7, pp. 3109–3121, Jul. 2017.

[29] J. Banfi, A. Quattrini Li, I. Rekleitis, F. Amigoni, and N. Basilico, "Strategies for coordinated multirobot exploration with recurrent connectivity constraints," *Auton. Robots*, vol. 42, no. 4, pp. 875–894, 2018.

[30] S. I. Roumeliotis and I. M. Rekleitis, "Analysis of multirobot localization uncertainty propagation," in *Proc. IEEE/RSJ Int. Conf. Intell. Robots Syst.*, vol. 2, 2003, pp. 1763–1770.

[31] A. I. Mourikis and S. I. Roumeliotis, "Performance analysis of multirobot cooperative localization," *IEEE Trans. Robot.*, vol. 22, no. 4, pp. 666–681, Aug. 2006.

[32] R. Kurazume and S. Hirose, "An experimental study of a cooperative positioning system," *Auton. Robots*, vol. 8, no. 1, pp. 43–52, 2000.

[33] N. Trawny and T. Barfoot, "Optimized motion strategies for cooperative localization of mobile robots," in *Proc. IEEE Int. Conf. Robot. Automat.*, 2004, pp. 1027–1032.

[34] Y. Shen and M. Z. Win, "Fundamental limits of wideband localization–Part I: A general framework," *IEEE Trans. Inf. Theory*, vol. 56, no. 10, pp. 4956–4980, Nov. 2010.

[35] Y. Shen, H. Wymeersch, and M. Z. Win, "Fundamental limits of wideband localization–Part II: Cooperative networks," *IEEE Trans. Inf. Theory*, vol. 56, no. 10, pp. 4981–5000, Oct. 2010.
[36] R. W. Cottle, "Manifestations of the Schur complement," *Linear Algebra Appl.*, vol. 8, no. 3, pp. 189–211, 1974.
[37] K. Zhou and S. I. Roumeliotis, "Multirobot active target tracking with combinations of relative observations," *IEEE Trans. Robot.*, vol. 27, no. 4, pp. 678–695, Aug. 2011.
[38] A. I. Mourikis and S. I. Roumeliotis, "Optimal sensor scheduling for resource-constrained localization of mobile robot formations," *IEEE Trans. Robot.*, vol. 22, no. 5, pp. 917–931, Oct. 2006.
[39] M. Z. Win, W. Dai, Y. Shen, G. Chrisikos, and H. V. Poor, "Network operation strategies for efficient localization and navigation," in *Proc. IRE*, vol. 106, no. 7, pp. 1224–1254, Jul. 2018.
[40] D. Levine, B. Luders, and J. P. How, "Information-theoretic motion planning for constrained sensor networks," *J. Aerosp. Inf. Syst.*, vol. 10, no. 10, pp. 476–496, 2013.
[41] M. Zhong and C. G. Cassandras, "Distributed coverage control and data collection with mobile sensor networks," *IEEE Trans. Autom. Control*, vol. 56, no. 10, pp. 2445–2455, Oct. 2011.
[42] T. Regev and V. Indelman, "Multi-robot decentralized belief space planning in unknown environments via efficient re-evaluation of impacted paths," in *Proc. IEEE/RSJ Int. Conf. Intell. Robots Syst.*, 2016, pp. 5591–5598.
[43] T. Regev and V. Indelman, "Decentralized multi-robot belief space planning in unknown environments via identification and efficient re-evaluation of impacted paths," *Auton. Robots*, vol. 42, no. 4, pp. 691–713, 2018.
[44] S. Thrun, "Probabilistic robotics," *Commun. ACM*, vol. 45, no. 3, pp. 52–57, 2002.
[45] S. Kotz, N. L. Johnson, and D. Boyd, "Series representations of distributions of quadratic forms in normal variables. I. Central case," *Ann. Math. Statist.*, vol. 38, no. 3, pp. 823–837, 1967.
[46] S. Kotz, N. L. Johnson, and D. Boyd, "Series representations of distributions of quadratic forms in normal variables II. Non-central case," *Ann. Math. Statist.*, vol. 38, no. 3, pp. 838–848, 1967.
[47] P. Patnaik, "The non-central χ 2-and F-distribution and their applications," *Biometrika*, vol. 36, no. 1/2, pp. 202–232, 1949.
[48] J.-P. Imhof, "Computing the distribution of quadratic forms in normal variables," *Biometrika*, vol. 48, no. 3/4, pp. 419–426, 1961.

Liang Zhang (Member, IEEE) received the B.Sc. degree in automation from Shandong University, Jinan, China, in 2015 and the Ph.D. degree in aeronautical and astronautical science and technology from the School of Astronautics, Harbin Institute of Technology, Harbin, China, in 2021. He was also a visiting Ph.D. student in the Autonomous System Lab, ETH Zürich, Switzerland, from 2018 to 2019 under the foundation from China Scholarship Council.

He is currently a Lecturer in the School of Engineering and Automation, Anhui University, China. His research interests are mainly around the multi-robot or multi-agent system (MAS/MRS), including cooperative control, planning under uncertainty and coverage control.

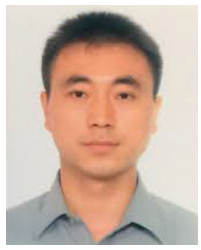

Zexu Zhang received the master's degree in signal and information processing and the Ph.D. degree in pattern recognition and intelligent systems from Harbin Institute of Technology, Harbin, China, in 2000 and 2004, respectively.

He is a Full Professor with the Harbin Institute of Technology, Harbin, where he is also the Director of the Institute of Aircraft Dynamics and Control. His research interests include aircraft autonomous navigation and control, intelligent cooperative perception and autonomous decision-making in drone swarm, data visualization. He was the Director of the Committee of Space Intelligence of the Chinese Society of Space Research (2021-2025).

Roland Siegwart (Fellow, IEEE) received the Diploma degree in mechanical engineering and the Ph.D. degree from ETH Zurich, Zurich, Switzerland, in 1983 and 1989, respectively.

He is a Professor for autonomous mobile robots with ETH Zurich, Zurich, Switzerland, the Founding Co-Director of the Technology Transfer Center, Wyss Zurich, and a Board Member of multiple high-tech companies. From 1996 to 2006, he was a Professor with EPFL Lausanne, held visiting positions with Stanford University and NASA Ames, and was the Vice President of ETH Zurich from 2010 to 2014. His research interest include the design, control, and navigation of flying, and wheeled and walking robots operating in complex and highly dynamical environments.

Prof. Siegwart received the IEEE RAS Pioneer Award and IEEE RAS Inaba Technical Award. He is among the most cited scientist in robots world-wide, Co-Founder of more than half a dozen spin-off companies, and a strong promoter of innovation and entrepreneurship in Switzerland.

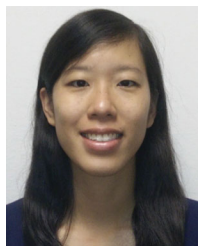

Jen Jen Chung (Member, IEEE) received the B.E. and the Ph.D. degrees in field robotics from the University of Sydney, Sydney, Australia, in 2014 and 2010, respectively.

She is a Senior Researcher in the Autonomous Systems Lab (ASL) at ETH Zürich. Her current research interests include perception and learning for mobile manipulation, algorithms for robot navigation through crowds, informative path planning and adaptive sampling. Prior to working at ASL, she was a postdoctoral scholar at Oregon State University researching multiagent learning methods and she completed her Ph.D. on information-based exploration-exploitation strategies for autonomous soaring platforms at the Australian Centre for Field Robotics in the University of Sydney.